Major role of shear heating in intracontinental inverted metamorphism: Inference from a thermo-kinematic parametric study

Sylvia Duprat-Oualid, Philippe Yamato, Pavel Pitra

▶ To cite this version:

Major role of shear heating in intracontinental inverted metamorphism:

Inference from a thermo-kinematic parametric study.

S. Duprat-Oualid[1, *], P. Yamato[1, 2] and P. Pitra[1]

[1]Géosciences Rennes, UMR6118, Université de Rennes 1 & CNRS, 35042 Rennes,

France

[2]ETH-Zurich, Sonneggstrasse 5, CH-8092 Zurich, Switzerland

[*]corresponding author: sylvia.duprat-oualid@univ-rennes1.fr

Reference:

Duprat-Oualid, S., Yamato, P. and Pitra, P., 2013. Major role of shear heating in intracontinental inverted metamorphism: Inference from a thermo-kinematic parametric study. Tectonophysics (in press), doi:10.1016/j.tecto.2013.07.037.

Available at: http://www.sciencedirect.com/science/article/pii/S0040195113004782.

Abstract

Inverted metamorphism corresponds to the stacking of high-temperature metamorphic units structurally on top of lower-temperature units and is commonly observed along main thrusts in major orogens. Yet, in spite of many existing models, the origin and preservation of the metamorphic inversion in intracontinental collision belts is still debated. In this study, we use a crustal-scale 2D thermo-kinematic model in order to investigate the key parameters controlling the inversion of the geothermal gradient at crustal scale. Our results confirm that the kinematic framework strongly impacts the thermal evolution around the thrust. Erosion velocity and thermal conductivity of rocks are two parameters that control the spatial location of the thermal perturbation and the intensity of inversion, respectively. However, even in extreme kinematic configurations, i.e., convergence velocities > 3cm.yr^{-1} and relatively high thrust dip angles ~ 30˚, the thermal inversion is fleeting and thrust temperatures cannot reach the high temperature peak values characteristic of natural occurences (> 600˚C) if shear heating is not taken into account. Conversion of mechanical energy into heat represents a main contribution to the thermal budget along main crustal shear zones. It leads to high temperature conditions in the thrust zone and our results attest that it is the only process that allows the preservation through time of an intense thermal inversion. Our quantification shows that shear heating is much more efficient than other processes such as accretion and surface denudation and is compatible with the observations of inverted metamorphism in the Himalayan or Variscan belts, for example. This comparison with natural occurrences suggests that the formation and preservation of intracontinental inverted metamorphism require shear zone viscosity values of the order of 10^{20}-10^{21} Pa.s for convergence velocities between 1 and 3 cm.yr^{-1}.

1. Introduction and state of the art

An inverted metamorphic sequence is characterised by an upward intensification of metamorphism, typically an increase of the metamorphic peak temperature. Inverted metamorphism is mostly related to major thrusts, where convergence velocities are high. The major occurrences can be ascribed to one of three distinct geological contexts: (i) metamorphic soles beneath ophiolites (e.g., Williams and Smyth, 1973; Jamieson, 1986; Hacker, 1991; Abd El-Naby et al., 2000); (ii) oceanic subduction zones (e.g., Toksöz et al., 1971; Platt, 1975); (iii) major thrusts in continental collision (e.g., LeFort, 1975; Kohn, 2008).

The present study is focused on the third geological setting. The best documented example is the inverted metamorphic sequence associated with the Main Central Thrust (MCT) zone in the southern Himalayas (e.g., Frank et al., 1973; LeFort, 1975; Sinha-Roy, 1982; Arita, 1983; Hubbard, 1989; Jain and Manickavasagam, 1993; Henry et al., 1997; Harrison et al., 1997, 1998, 1999; Caddick et al., 2007; Kohn, 2008), but other examples were described in the Variscan belt (Burg et al., 1984; Arenas et al., 1995; Štípská and Schulmann, 1995; Ballèvre et al., 2009; Pitra et al., 2010), in the Caledonian belt (Andreasson and Lagerblad, 1980; Mason, 1984; Watkins, 1985; Johnson and Strachan, 2006) or in the Appalachian belt (Camiré, 1995). The pressure and temperature conditions within such thrust zones attest to a medium pressure, medium-high temperature metamorphism. As an example, inverted metamorphic sequences in both the Himalayas and the Variscan belt have recorded peak temperatures between 500 and 700°C and peak pressures between 8 and 11 kbar (e.g., Burg et al., 1984; Macfarlane, 1995; Guillot, 1999; Kohn, 2008; Pitra et al., 2010; Corrie and Kohn, 2011). Natural intracontinental metamorphic inversions are thus characterised by inverted thermal gradients between 10 and 50°C.km^{-1} (e.g., Kohn, 2008; Pitra et al., 2010). Such intense thermal perturbations over a thickness of several kilometres necessarily imply geodynamic processes at crustal or even lithospheric scale. Several numerical models have

been developed, most of them constrained by or aiming to fit data from the Himalayan belt (e.g., Jamieson et al., 1996, 2004; Henry et al., 1997; Bollinger et al., 2006; Kohn, 2008). They suggest two alternative hypotheses to explain the metamorphic inversion.

On the one hand, the inverted zonation is the result of a post-metamorphic deformation of a preexisting "normal" metamorphic sequence. This may result from late thrusts cutting through the initial metamorphic sequence (e.g., Brunel and Kienast, 1986), passive deformation of metamorphic isograds within a ductile shear zone (e.g., Jain and Manickavasagam, 1993; Grujic et al., 1996; Gibson et al., 1999) or crustal-scale folding (e.g., Searle and Rex, 1989; Stephenson et al., 2000).

On the other hand, the inverted zonation may result from a temporary spatial perturbation of crustal isotherms (LeFort, 1975; Peacock, 1987a; Jamieson et al., 1996, 2004; Burg and Schmalholz, 2008). In this hypothesis, metamorphism is synchronous with the deformation event. Some authors propose that inverted metamorphism occurs due to a diffusive heat transfer across the major thrust from the hotter upper unit to the colder subjacent unit (e.g., LeFort, 1975; Shi and Wang, 1987; England and Molnar, 1993). Particularly, the thermal inversion may be due to a "channel flow", i.e., the extrusion of deep hot crustal rocks above a colder plate (e.g., Grujic et al., 1996; Jamieson et al., 1996, 2004). This model presents the advantage of reproducing the ranges of metamorphic pressures and temperatures characterising the outcroping sections of the MCT (Beaumont et al., 2001). However, it requires strong erosion localised on the thrust front and specific internal physical properties in terms of viscosity and angle of friction. Furthermore, it fails to reproduce some important metamorphic and geochronological records on both sides of the MCT (Kohn, 2008).

Beyond the first-order role of the kinematic framework and thermal diffusion, several studies have specifically focused on the contribution of radiogenic heat, including the

accretion of radioactive material across the active thrust, and on the role of erosion (Royden, 1993; Ruppel and Hodges, 1994; Huerta et al., 1996, 1998, 1999; Bollinger et al., 2006). Accretion models allowing the accumulation of highly radioactive material over a duration longer than 30 Myr can lead to significant increase of temperature within the hanging wall (e.g., Huerta et al., 1996, 1998). However, such studies involve disputable initial assumptions. As an example, the orogenic accretionary wedges of these models (e.g., Huerta et al., 1998) are deeply rooted at 30 to 60 km depths. Reasonable accretion velocities associated with lower, realistic erosion velocities lead to wedges several hundreds of kilometers wide at the surface. Outcrouping rocks across such wide zones should consequently be characterised by a continuous intense deformation and none of the known frontal thrusts displays a such configuration. Moreover, in most cases, strong accretion alone cannot reproduce the high temperatures observed in natural inverted metamorphic sequences. On the contrary, accretion leads to progressive cooling of the active thrust plane to steady temperatures lower than 400°C at 30 km depth with no significant thermal inversion (Royden, 1993). Concomitant surface denudation characterised by an erosion velocity greater than the accretion velocity is necessary to raise the temperatures in the thrust zones (e.g., Royden, 1993; Bollinger et al., 2006).

In the absence of accretion processes, moderate erosion velocities can lead to thrust temperatures of the order of 600°C and to the development of inverted isotherms comparable to those observed in natural inverted metamorphic sequences (Royden, 1993). However, these conclusions require a thrust activity lasting for more than 70 Myr and exhumation of ultra-high pressure metamorphic rocks from more than 100 km depth (Royden, 1993). Such implications are not compatible with natural cases where rocks recorded metamorphic peak pressures of 8 to 11 kbar. From a mechanical approach, erosion catalyses the development of main orogenic structures (e.g., Burg and Schmalholz, 2008), and some models highlight the

important influence of both the erosion and the exhumation on the thermal perturbation (e.g., Jamieson et al., 1996; Beaumont et al., 2004; Bollinger et al., 2006; Kohn, 2008).

The role of heat production by conversion of mechanical energy into thermal energy in a major shear zone (shear heating) was also considered to complete the thermal budget and the possible development of thermal inversion around a thrust (Minear and Toksöz, 1970; Toksöz et al., 1971; LeFort, 1975; Graham and England, 1976; Scholz, 1980; England and Thompson, 1984; Pavlis, 1986; Molnar and England, 1990; England and Molnar, 1993; Burg and Gerya, 2005; Burg and Schmalholz, 2008), but without real quantification. Kidder et al. (2013) specifically refute the importance of shear heating under high convergence velocity ($\sim$10 cm.yr^{-1}) and attribute the thermal inversion to accretion process.

The demonstration provided by Kidder et al. (2013) that shear heating is not a cause of inverted metamorphism in accretion domains is based on an oceanic subduction beneath an active arc (Kidder and Ducea, 2006). The very high convergence velocity ($\sim$10 cm.yr^{-1}) and the high initial geothermal gradients characterising the overriding forearc (Kidder and Ducea, 2006) and the subducting oceanic plate easily and rapidly lead to intense thermal inversion. With low shear heating ($\sim$10^{-5} W.m^{-3} implying very low viscosities of about 10^{17} Pa.s), heat advection and conduction dominate the thermal budget: both the overriding plate and the slab are rapidly cooled and the subducting material is progressively and slowly heated. Consequently, the rocks accumulated in the accretion zone are representative of the thermal state of the thrust plane. Understandingly, the thermal peaks are thus colder from the top to the base of the accretion area and such thermal inversion is compatible with the thermochronologic data from the Pelona Schist of southern California (Kidder et al., 2013). Considering a stronger shear heating along the active thrust, which is superposed on the overall cooling pattern, decreases the thermal inversion intensity recorded in the accreted sediments. Nevertheless, such shear heating assumptions are not generally applicable because

very low shear stress and viscosities are involved to balance the high strain rate (10^{-12} to 10^{-11} s^{-1}).

Previous studies of syn-deformational intracontinental inverted metamorphism used various models with very different degrees of complexity (e.g., Shi and Wang, 1987; England and Molnar, 1993; Jamieson et al., 2004). However, none of the proposed models is commonly accepted to give a general explanation to the development of syn-deformation inverted metamorphism. Whereas analytical studies provide good mathematical solutions for understanding the respective influence of kinematics and heat diffusion on the thermal evolution, the other factors involved (e.g., erosion, various heat sources, variable kinematic configuration, thermo-dependence laws) are difficult to address analytically but can be solved and quantified numerically.

In the present paper, our goal is not to fit a particular natural case (e.g., the Himalayas). Rather, using a systematic approach, we aim to explore and provide a detailed synthesis of the different conditions required for the formation and preservation of crustal-scale inverted metamorphism along one intracontinental thrust. We define and compare the relative importance of each one of the parameters and processes involved: kinematic setting, thrust geometry, erosion velocity, rock properties (in particular the thermal diffusivity), accretion velocity, radiogenic heat production and shear heating. The goal is to infer (i) the conditions required to locally invert the thermal field; (ii) the exact impact of each one of these parameters on the intensity, the location and the duration of the inversion and (iii) the conditions required to preserve the thermal inversion through time. Finally, we discuss how and why shear heating is crucial for the formation and preservation of inverted thermal gradients under realistic kinematic settings.

2. Numerical model

2.1. Initial setup

In order to test independently the influence of the various parameters and processes on the thermal evolution of a crustal thrust, a simple numerical model is defined in which each component can be controlled. The 2D-model setup (Fig. 1a) is focused on the first 80 km of a continental lithosphere, which includes a 30 km thick crust. In order to study the thermal evolution of a major continental thrust zone, a thrust cutting through the whole continental crust with a dip angle θ is simulated by imposing a velocity contrast between the downgoing plate and the upper plate, moving with a velocity V_{lp} and V_{up}, respectively (Fig. 1). The convergence velocity V_{th} is consequently given by $V_{th} = V_{lp} + V_{up}$. The thrust is mainly represented by a straight segment, the dip angle of which, however, progressively decreases towards both the base of the crust and the surface in order to avoid any advection errors due to local strong velocity direction contrasts. Since the present study focuses on the slanted part of the thrust and because the temperature evolution around the thrust and in the deepest levels of the fault is not noticeably affected by the configuration of the lower block velocity field beneath the first 30 km (see Appendix A, Fig. A.1), the downgoing plate intentionally lies flat under the upper crust to simplify the boundary conditions and the isostasy computation.

The initial geotherm is defined in the whole model according to the following equation:

$$T(x,z,t_0) = T_{surface} + z \cdot \frac{q_{base}}{k} + T_{source}(x,z) \tag{1}$$

where $T_{surface}$, q_{base}, k and T_{source} are the surface temperature, the mantle heat flux, the thermal conductivity and the possible local heat sources, respectively. Initially, the only implemented heat source is the radiogenic heat production. It is considered as a permanent property of the

9

material and is defined according to the following decreasing exponential law from Turcotte and Schubert (2002):

$$Q(z,t_0) = Q_0 + \exp\left(\frac{-z}{z_r}\right) \tag{2}$$

where Q_0 is the surface radiogenic heat production, and z_r corresponds to the length scale for the decrease in Q with depth (Turcotte and Schubert, 2002) controlling the curvature of the vertical profile of Q. Eq. (2) allows to easily test a wide range of possible distributions of radiogenic production and both parameters Q_0 and z_r, were independently tested. In the presence of radiogenic heat sources, Eq. (1) is then only z-dependent and becomes:

$$T(z,t_0) = T_{surface} + z \cdot \frac{q_{base}}{k} + \frac{Q_0 \cdot z_r^{\,2}}{k} \cdot \left(1 - \exp\left(\frac{-z}{z_r}\right)\right) \tag{3}$$

2.2. Computation methods

Both kinematic and thermal computations are based on a regular Eulerian grid with a space resolution of 1 km. During the thrust activity, at each time step, advection and thermal diffusion are realised separately in order to minimise the numerical diffusion of temperature inside a non-static environment by using the marker-in-cells method (Gerya, 2010). The advection of rock properties and temperature is ensured by a field of initially randomly distributed particles (see Appendix A for more details). Three kinematic parameters can be distinguished here (Fig. 1b). The first one is the burial velocity Vb of the downgoing plate corresponding to the vertical component of the velocity field V_{lp} and defined by:

$$Vb = V_{lp} \cdot \sin(\theta) \tag{4}$$

The second parameter defines the vertical accretion velocity *a*. As in previous studies (e.g., Royden, 1993; Huerta et al., 1996, 1998, 1999), accretion is realised at each time step by adding a horizontal velocity component *a'* (Fig. 1b) in the whole model so that both the active thrust position and the convergence velocity remain fixed. Both parameters are related according to:

$$a' = a \cdot \tan(\theta) \tag{5}$$

The third kinematic parameter corresponds to the maximum erosion velocity *Ve* linked to the upper plate velocity V_{up} by the following equation:

$$Ve = V_{up} \cdot \sin(\theta) \tag{6}$$

The erosion velocity *Ve* controls the upper plate velocity V_{up} in the models (Fig. 1b, see Appendix A for more details).

Compared to the tectonic advection times, the isostatic balance is reached instantaneously (Crough, 1977). Thus, at each time step, the isostatic response is calculated in the entire model thereby producing a realistic topography associated with the thrust.

Then, for the thermal part, the following heat equation is solved by using the implicit finite difference method on the Eulerian grid. In order to limit numerical diffusion, the Eulerian computation is coupled with intermediate thermal interpolations with the Lagrangian particles (see Appendix A for more details):

$$\rho \cdot Cp \cdot \frac{\partial T}{\partial t} - \frac{\partial}{\partial x}\left(k\frac{\partial T}{\partial x}\right) - \frac{\partial}{\partial z}\left(k\frac{\partial T}{\partial z}\right) = Q + Hs \tag{7}$$

11

The heat equation (Eq. (7)) is composed by a heat diffusion part where ρ, Cp and k are respectively the density, the heat capacity and the thermal conductivity (left side of Eq. (7)) and by a heat production part (right side of Eq. (7)) where Q and Hs represent the radiogenic heat production and the shear heating, respectively.

The parameters ρ, Cp, and k define the capacity of the material to diffuse heat. This property can be reduced to one parameter, the thermal diffusivity κ, defined as $\kappa = k/(\rho.Cp)$. Each one of these three parameters depends on the lithology, but also on the physical environment of the rock (e.g., pressure, temperature). Various empirical laws describe the temperature and pressure dependence of these parameters in rocks (e.g., Zoth and Hänel, 1988; Seipold, 1995, 1998; Abdulagatov et al., 2006; Hofmeister, 2007; Whittington et al., 2009). In the present study, we tested independently the influence of a range of realistic values for each parameter on the thermal evolution around the thrust (see Table 1). First, these values were considered constant in the crust and in the mantle. In a second time, their temperature and pressure dependence is considered and their influence on the thermal field investigated. These results are discussed in section 3.3.2.

Shear heating Hs results from the transformation of mechanical energy into heat during deformation and is recognised as a major component of the total energy budget (e.g., Brun and Cobbold, 1980; Lachenbruch and Sass, 1980; Chester et al., 2005). Shear heating is a function of the strain rate and stress tensors ($\dot{\varepsilon}_{ij}$ and σ_{ij} respectively) and is computed according to the following equation:

$$Hs = \sigma_{xx} \cdot \dot{\varepsilon}_{xx} + \sigma_{zz} \cdot \dot{\varepsilon}_{zz} + 2 \cdot \sigma_{xz} \cdot \dot{\varepsilon}_{xz} \tag{8}$$

The strain rate tensor is defined as $\dot{\varepsilon}_{ij} = 0.5\ [(\partial V_i/\partial j) + (\partial V_j/\partial i)]$ where $\partial V_i/\partial j$ corresponds to the variation of the velocity of the component i in the direction j and the same convention applies for $\partial V_j/\partial i$. Because shear zones related to inverted metamorphism can be several kilometres thick (e.g., Grugic et al., 1996), ductile rheology is generally attributed to the whole thrust (e.g., Searle and Rex, 1989; Jamieson et al., 1996; Kidder and Ducea, 2006). In the present study, the shear zone thickness is space resolution dependent and is thus approximately of about 1 km. Shear heating is computed in a ductile manner, where stress and strain rate are linked by the effective viscosity η of the material constituting the thrust:

$$\sigma_{ij} = 2 \cdot \eta \cdot \dot{\varepsilon}_{ij} \tag{9}$$

Viscosity depends on temperature, strain rate and creep parameters (e.g., Goetze and Evans, 1979; Carter and Tsenn, 1987; Ranalli and Murphy, 1987). It tends to decrease with increasing strain rate and temperature (Meissner and Mooney, 1998). Inversely, both the rock deformation and the associated shear heating depend on the viscosity (e.g., Burg and Schmalholz, 2008; Hartz and Podladchikov, 2008). However, in order to better define the first order role of viscosity, we simplified the problem by using a constant viscosity η all within the thrust (see discussion in section 3.4).

3. Model results

3.1. Burial velocity effects

In order to test the validity of our numerical model, we first realised a comparative study with analytical solutions from England and Molnar (1993). The results are described in Appendix B.

In extreme kinematic configurations (e.g., V_{th} = 5 cm.yr^{-1}, θ = 30˚), which favour the development of thermal inversion, the thermal evolution around the thrust and in the whole model can be best characterised. In this case, because the initial geotherm is linear, the thermal inversion starts on a large part of the thrust with a relatively homogeneous intensity. Then, the affected area progressively deepens and widens and the maximum intensity is localised towards the deepest levels of the thrust. On each point of the thrust, the vertical temperature gradient $\partial T / \partial z$ first decreases, reaches a minimum value (negative when thermal inversion occurs) and then increases again until a steady state when the temperature advection and the heat diffusion are completely balanced. Nevertheless, even under such extreme kinematic settings, none of the (V_{th}, θ) combinations allows the preservation of the thermal inversion in time beyond the first 6 Myr (see Appendix B, Fig. B.2).

3.2. Erosion effects

In our model, erosion can be activated and is only controlled by the erosion velocity Ve (Eq. (6), Fig. 1 and Table 1). In this case, contrary to the previous analysis (section 3.1, Appendix B), the thrust velocity V_{th} is given by a combination of the lower and the upper plates velocities (V_{lp} and V_{up}, see Fig. 1b). Consequently, in order to test the influence of the erosion velocity independently of the kinematic setting, either the downgoing plate velocity V_{lp} or the thrust velocity V_{th} have to be fixed. Here, we chose to keep constant the thrust velocity V_{th} for two reasons. (i) Kinematic simulations having the same vertical component Vz of the thrust velocity (Fig. 1b) are characterised by very similar thermal evolutions (see Appendix B). Each given Vz value corresponds to a group of (V_{th}, θ) combinations. This allows us to easily make connections and distinctions between the thermal evolution around the thrust and, on the one hand, the erosion velocity, and on the other hand, the convergence velocity and the thrust dip angle. In comparison with the MCT in the Himalayas which is

characterised by a high downgoing velocity of the Indian plate of ~ 2 cm.yr^{-1} for the last 10 to 20 Myr (e.g., Bilham et al., 1997; Lavé and Avouac, 2000) and a dip angle of ~ 15˚ (e.g., Kaneko et al., 2003), Vz values of the order of 0.5 cm.yr^{-1} are realistic and greater values are excessive. (ii) A further parametric analysis concerning the shear heating (section 3.4) takes into account the velocity contrast on the thrust as a major parameter. Controlling the thrust velocity instead of the downgoing plate velocity is thus more practical to compare the combined effects of the kinematic setting, the erosion velocity and the shear heating. The distribution of the velocity field on both sides of the thrust can be described as the ratio between the erosion velocity Ve and the vertical component Vz of the thrust velocity (see Fig. 1).

Erosion and motion of the upper plate, for a constant V_{th}, does not lead to significant variations of the reached intensity (Fig. 2a) and of the thickness of the affected area (Fig. 2b) of the thermal inversion during the thrust activity. However, it strongly influences its space and time locations. Increasing erosion and hence displacement of the upper plate tends to localise the thermal inversion at shallower depths along the thrust (Fig. 2). Taking out crustal material by erosion leads to progressive cooling of the remaining shallowest material controlled by surface thermal conditions. The maximum thermal inversion intensity is not restricted to the base of the slanted part of the thrust but moves to the surface with increasing erosion velocities. However, because erosion velocities are not sufficiently high to efficiently balance the thermal diffusion, even for extreme cases, thermal inversion cannot occur at very superficial levels along the thrust.

The time of maximum inversion is not significantly changed, even if a slight delay can be noticed. The duration of the thermal inversion is widely extended with erosion. However, if for extreme kinematic and erosion values thermal inversion can be preserved until the

steady state, the most realistic kinematic setting tested (corresponding to $Vz = 0.5$ cm.yr^{-1}) never leads to a thermal inversion, whatever the applied erosion velocity (Fig. 2).

Hence, when the displacement along the thrust is entirely ensured by the downgoing plate ($Ve = 0$), temperature on each point along the thrust is continually decreasing until the steady state. When the upper plate velocity V_{up} approximates the lower plate velocity V_{lp}, (i.e., $Ve \approx 0.5Vz$), the thermal evolution along the thrust tends to be reversed. Thus, for $Ve > 0.5Vz$, temperature at a given point of the thrust starts to increase in the beginning of the thrust activity (Fig. 2a, case $Ve = 2Vz/3$) due to the fast exhumation of the deep hot portions of the upper plate. This trend increases with the vertical component Vz of the thrust velocity. After reaching a local temperature peak, maximum thermal inversion is quickly reached and the temperature along the whole thrust decreases until the steady state. Actually, the thrust profile flattening in depth limits the temperature increase because the deepest rocks involved in the thrust come from the base of the upper continental block and cannot thus be hotter than the initial Moho temperature.

To summarise, erosion tends to localise the thermal inversion towards shallower depths of the thrust and significantly increases the thermal inversion duration. Nevertheless, it does not affect the intensity and the thickness of the thermal inversion. Furthermore, even in extreme cases, the initial temperature increase on the thrust is limited (maximum 25˚C) and is far from sufficient to account for the high temperatures known in major thrust zones associated with inverted metamorphism.

3.3. Rock properties effects

In the lithosphere, conduction is generally the predominant heat transport mechanism ahead of convection and radiation (Lachenbruch and Sass, 1980; Abdulagatov et al. 2006). As shown previously in section 2.2, ρ, Cp and k constitute the three rocks properties involved in

the heat diffusion equation. Moreover, as defined by Eq. (3), the initial geotherm in the lithosphere is not only controlled by k and the radiogenic heat sources, but also by the basal mantle heat flux q_{base}. These thermal parameters are here considered independently and the impact of the radioactive character of the crust on the thermal evolution around the thrust is also discussed.

3.3.1. Heat diffusion properties and the mantle heat flux

The ranges of realistic values (Table 1) for each thermal parameter depend strongly on the lithology. On the one hand, the k values are generally comprised between 2 $W.m^{-1}.K^{-1}$ and 4 $W.m^{-1}.K^{-1}$ (Clauser and Huenges, 1995; Turcotte and Schubert, 2002). This high degree of variability of more than 100 % proportionally controls the thermal diffusivity κ with the same order of magnitude. On the other hand, the heat capacity Cp varies up to ~ 50 %, from 800 to 1200 $J.kg^{-1}.K^{-1}$ (Waples and Waples, 2004), involving maximum differences for κ of ~ 30 %. Depending on the lithology, the crustal rock density ρ varies from ~ 2400 $kg.m^{-3}$ for sedimentary rocks to ~3300 $kg.m^{-3}$ for basic eclogites as an extreme case, but is generally comprised between 2500 and 3000 $kg.m^{-3}$ with an associated variability of ~ 20%. Heat diffusion is therefore mainly controlled by the variation of thermal conductivity, and the influence of the variations of density and heat capacity are less significant (see Appendix C, Fig. C.1). This has two reasons:

First, the hotter is the geotherm (obtained for a low thermal conductivity in the crust or a high mantle heat flux), the higher is the thermal inversion (Fig, 3a, c). The basal heat flux, q_{base}, only involved in the initial and boundary conditions, influences the intensity of the thermal inversion proportionally to the magnitude of its variability. For example, between q_{base} = 20 $mW.m^{-2}$ and q_{base} = 40 $mW.m^{-2}$, the initial thermal gradient is two times higher and the thermal inversion intensity reached on each point of the thrust is doubled (Fig. 3c).

Proportionally to a q_{base} increase, the intensification of the inversion with decreasing k is more significant. From $k = 3$ to 2 W.m^{-1}.K^{-1}, the thermal inversion is approximately two times higher (Fig. 3a). Thus, the initial thermal structure of the lithosphere, defined by the distribution of both q_{base} and k, constitutes a key parameter controlling the intensity reached by the thermal inversion. Nevertheless, the location of the inversion, both in space and time, is mostly insensitive to either q_{base} or k (Fig. 3).

Second, the strong correlation between κ and k leads the latter to strongly influence the heat diffusion through the thrust. A low thermal conductivity decreases the heat diffusion and thus favours thermal inversion during thrusting. For this reason, the influence of both k and q_{base} on the thermal evolution around the thrust is different (Fig. 3). A decrease of k induces a more significant intensification of the inversion than an increase of q_{base} (Fig. 3a, c). Furthermore, contrary to the intensification of the basal heat flux, a decrease of k induces a widening of the thrust part affected by the inversion, a thickening of the area where the thermal inversion occurs (Fig. 3b, d) and a continuation in time of the thermal inversion (Fig. 3).

3.3.2. Temperature and pressure dependences

Thermal properties also vary as a function of temperature and pressure. Various experiments have been realised and some empirical laws have been proposed in order to define the thermal dependence of the thermal conductivity k (Zoth and Hänel, 1988; Horai and Susaki, 1989; Clauser and Huenges, 1995; Seipold, 1998; Voosten and Schellschmidt, 2003; Abdulagatov et al., 2006; Whittington et al., 2009) and heat capacity Cp (Waples and Waples, 2004; Whittington et al., 2009). Generally, with increasing temperature, k decreases, whereas Cp increases. Conversely, thermal conductivity tends to increase with increasing pressure (Horai and Susaki, 1989; Seipold, 1992, Kukkonen et al., 1999; Osako et al., 2004;

Abdulagatov et al., 2006; Hofmeister, 2007). However, the pressure effect is limited compared to the influence of temperature (Abdulagatov et al., 2006).

The reported variation of each thermal property as a function of temperature and pressure lies within the range of constant values tested in our numerical simulations (Table 1). Only the variability of k has a significant impact on the thermal evolution around the thrust. However, k depends on both the lithology and the physical environment, and this impact is difficult to quantify. Indeed, in spite of the numerous laboratory experiments (e.g., Čermák and Rybach, 1982; Osako et al., 2004; Abdulagatov et al., 2006), none of the proposed empiric laws (Zoth and Hänel, 1988; Clauser and Huenges, 1995; Seipold, 1998; Voosten and Schellschmidt, 2003; Abdulagatov et al., 2006; Whittington et al., 2009) appears to be undisputable (Fig. 4). Diverse equations relative to the same lithology appear inconsistent with one another (Fig. 4c, d). Furthermore, they are associated with large uncertainties (e.g., Seipold, 1998, Fig. 4a) and rarely integrate both temperature and pressure dependences in the same time (Kukkonen et al., 1999; Abdulagatov et al., 2006).

Regarding only the vertical distribution of the theoretical lithologies (after Turcotte and Schubert, 2002), the thermal conductivity increases from the superficial levels (sediments) to the mantle rocks. On the other hand, within each lithology, k decreases significantly with temperature (and hence depth; Fig. 4). This progressive drop may reach 30-50 % from 0 to 600 ˚C. Concerning the pressure influence, k increases with depth in the shallowest crustal levels due to the reduction of the pore volume (Abdulagatov et al., 2006). Beyond ~ 100 MPa, k tends to reach a linear behaviour (Horai and Susaki, 1989; Clauser and Huenges, 1995; Abdulagatov et al., 2006), and is supposed to evolve following the thermo-dependence law appropriate for the considered lithology.

To sum up, within the range of realistic values, both Cp and ρ have negligible effects on the thermal evolution of the lithosphere, and the diffusive transport of heat is controlled by

the variability of k. The temperature and pressure dependences do not change the order of variability, but they can lead to different thermal behaviours inside the lithosphere (Maierová et al., 2012). In particular, the dependence of the k value on temperature for a given lithology and pressures > 100 MPa favours the thermal inversion in depths. These physical and lithologic dependences are generally not taken into account in the numerical models although the values allocated to the thermal conductivity have to be considered with caution (Nabelek et al., 2010).

3.3.3. Radiogenic heat production

As for the heat diffusion properties (section 3.3.1, Appendix C), numerical simulations were realised in an extreme kinematic context ($V_{th} = V_{lb} = 5$ cm.yr^{-1} and $\theta = 30°$) in order to quantify the effect of the radiogenic heat production. They show that although the radiogenic heat production contributes to the initial geothermal profile, it does not influence the thermal inversion around the thrust in terms of intensity and localisation (Appendix C, Fig. C.2).

The previous analysis revealed that the burial velocity, the erosion velocity and the thermal conductivity of rocks are the main parameters controlling the thermal evolution around a crustal scale thrust. Nevertheless, considering realistic kinematic settings (V_{th} < 3 cm.yr^{-1}), none of these parameters allows the preservation of an established thermal inversion in time.

3.4. Shear heating effects

Shear heating constitutes a part of the conservation of energy and a study of the thermal evolution around a thrust during its activity requires to take into account the relative displacement between the two crustal blocks as a source of heat (Toksöz et al., 1971; Brun and Cobbold, 1980; Pavlis, 1986). By considering shear heating in the viscous way, two

parameters have to be examined: the strain rate $\dot{\varepsilon}$ and the effective viscosity η within the thrust (section 2.2, Eq. (8) and (9)). Since the velocity field is not mechanically computed in our numerical models but imposed, both $\dot{\varepsilon}$ and η can be considered independently. The initial kinematic conditions used here are based on realistic cases for continental collision: the maximum dip angle θ of the thrust set to 15° and the velocity thrust values between 1 and 3 cm.yr^{-1}, implying strain rates from 3.10^{-13} to 10^{-12} s^{-1}.

In rocks, viscosity is temperature- and strain rate-dependent. Considering an undeformed crust, the viscosity field is characterised by a decrease from ~ 10^{25} Pa.s in the cold upper crust to ~ 10^{21} Pa.s in the hot lower crust (e.g., Burg and Gerya, 2005). The interdependence of strain rate and viscosity tends to a steady state and, as an example, with a convergence velocity of 2 cm.yr^{-1}, the viscosity drops to values of 10^{19} to 10^{21} Pa.s within major shear zones (Burg and Gerya, 2005). Consequently, we chose to apply this range of viscosity values, constant in time and space along the thrust. In our kinematic models, the strain field is only localised along the thrust (Fig. 1) thus limiting the frictional heat production to the shear zone. In order to highlight the effects of shear heating, no additional heat source is taken into account, and the erosion is not considered so that the downgoing plate only ensures the displacement along the thrust.

The theoretical amount of heat produced (Eq. (8)) along the thrust is very sensitive to even small variations of viscosity (Fig. 5c). Considering the lowest viscosity ($\eta = 10^{19}$ Pa.s) and strain rate ($\dot{\varepsilon} = 3.17 \cdot 10^{-13}$ s^{-1}), the resulting frictionnal heat produced ($Hs \approx 4$ μW.m^{-3}) is of the same order of magnitude as the maximum realistic radiogenic heat production (Table 1). A viscosity increase induces a proportional increase of shear heating along the thrust. For example, an increase of $10^{0.25}$ Pa.s will typically result in an elevation of ~ $10^{0.25} = 178$ % of the produced heat (Fig. 5c). This way, (i) shear heating can efficiently balance the diffusive cooling of the overriding plate. For high viscosity values, the thermal gradient above the

thrust can be elevated beyond the initial crustal geotherm. Consequently, if the heating produced by shearing becomes higher than the cooling driven by the underthrusting of cold material, the surface heat flow at the top of the upper block increases during thrusting (Hartz and Podladchikov, 2008). (ii) The thermal budget at the top of the downgoing crust has two sources: the transfer by diffusion of the heat inherited in the upper block and the shear heating along the thrust. Consequently, in presence of shear heating, the maximum thermal perturbation appears and develops under the thrust, whereas it straddles the thrust when shear heating is not considered (Fig. 5a, b).

As shown in Fig. 6, the amount of heat produced by shearing leads to an intense thermal inversion characterised by a significant thickening of the area affected and to a long duration. Unlike the other situations considered, shear heating allows the preservation of the thermal inversion in time until the steady state under realistic kinematic settings (V_{th} = 1-3 cm.yr^{-1}; Fig. 5b and 6).

Thermal inversion intensities, even at shallow depths, can exceed 100˚C.km^{-1} and temperatures extend up to more than 1000˚C (Fig. 7). Both ranges of temperatures between 500 and 700˚C and of thermal inversion intensities from 10 to 50˚C.km^{-1} are reached between 20 and 30 km depth for different combinations of viscosity and convergence velocity (Fig. 8). Consequently, shear heating alone can reproduce and preserve in time thermal features comparable to natural occurences of inverted metamorphic sequences. Furthermore, our model suggests that, in these cases, viscosity values within the thrust zone have to range between 10^{20} to 10^{21} Pa.s (Fig. 8).

In short, for small variations of viscosity or strain rate across a thrust (constant width of the sheared area), the thermal inversion is strongly influenced by shear heating in terms of intensity, space and time location. Although shear heating does not necessary imply an inversion, it plays a major role in the preservation of the perturbation in time.

3.5. Shear heating, accretion and radiogenic heat production competition

Accretion processes were implemented while keeping shear heating in action along the active thrust. As previously, the thrust dip angle θ was set to 15˚. The convergence velocity V_{th} was fixed at 2 cm.yr^{-1} and no erosion process was considered. The vertical accretion velocities a tested were 1 and 2 mm.yr^{-1} and are comparable to the values used in previous works (Royden, 1993; Huerta et al., 1996, 1998, 1999; Bollinger et al., 2006; Kidder et al., 2013). In order to evaluate the thermal influence of accumulation of radioactive material in the accretion prism, an elevated accretion velocity ($a = 2$ mm.yr^{-1}) was considered and two radiogenic profiles (Eq. (2) and (3)) characterised by a common surface radiogenic heat production $Q_0 = 2$ µW.m^{-3} but differing in the specific depth z_r were tested : (i) a realistic configuration with $z_r = 15$ km and (ii) an extreme case with $z_r = 30$ km such that the whole continental crust is highly enriched in radioactive elements. Mantle flux was adapted to each thermal configuration in order to ensure a realistic initial temperature at the base of the crust between 420 and 500˚C.

Results are synthesised in Fig. 9 in terms of maximum thermal inversion intensity and maximum temperatures reached in the thrust zone after the thermal steady state is attained. Whether we take into account accretion and radiogenic heat production or not, no significant thermal inversion occurs if the viscosity η is lower than $10^{20.25}$ Pa.s. Low viscosity implying low amounts of shear heating (Eq. (8) and (9)), it follows that, in the framework of realisitc kinematic and thermal settings, it is impossible to reproduce metamorphic inversions comparable to natural observations by considering accretion processes only. Conversely, if η exceeds 10^{21} Pa.s, temperatures and geothermal gradients within the thrust zone are excessively elevated whatever the depth considered. Thus, under a given kinematic context,

the range of viscosities leading to realistic thermal inversions is relatively narrow, of the order of 10^{20} to 10^{21} Pa.s (Fig. 8 and 9).

The concomitance of accretion and shear heating implies that material previously deformed and warmed within the thrust zone is accumulated in the hanging wall while subjacent volumes are in turn sheared and heated. For low amounts of shear heating, upward heat transfert by accretion leads to a smaller pertubation on the geothermal gradient around the active thrust (Fig. 9a) and no change in the maximum temperatures (Fig. 9b). Conversely, when shear heating is significant, accretion of hot material efficiently reduces the heat diffusion from the thrust zone to the overriding plate. Thermal inversion in the active thrust zone is consequently more intense and this trend is more pronounced in depth. However, because the material heated in the shear zone is continuously moved upwards out of the active shear zone, the maximum temperatures are significantly lower (e.g., about 50˚C lower with a 2 mm.yr^{-1} accretion velocity and $\eta = 10^{20.5}$ Pa.s. and almost 100˚C lower with a 1 mm.yr^{-1} accretion velocity and $\eta = 10^{20.75}$ Pa.s.) (Fig. 9b).

Accretion of radioactive material associated with shear heating has no significant effect on the maximum intensity of thermal inversion, even if extremely radioactive crustal material is considered (Fig. 9a). Because the top of the downgoing plate is highly radioactive, the maximum temperatures reached along the thrust are obviously hotter than without radiogenic heating.

In short, whatever the accretion velocity or the radiogenic heat production, even in extreme cases, none of these processes can lead to thermal inversion without shear heating in the framework of realistic kinematic and thermal settings. Furthermore, maximum thermal features in the thrust zone are more influenced by small viscosity variations than by high changes of the accretion velocity and of the amount of radiogenic heating.

3.6. Shear heating and erosion

On the one hand, surface denudation enhances the localisation of the thermal inversion at shallower depths and can lead to increased temperatures along the thrust (see section 3.2). On the other hand, shear heating strongly influences the crustal thermal budget and highly intensifies the thermal inversion (see sections 3.4 and 3.5). Consequently, numerical simulations taking into account both processes are necessary to complete our parametric study (Fig. 9). Here again, tests were performed with a thrust dipping 15° and a convergence velocity V_{th} of 2 cm.yr^{-1}. Accretion and radiogenic heat production were switched off. Viscosities ranged between 10^{19} and 10^{21} Pa.s and erosion velocity was set to $Ve = 2$ mm.yr^{-1}. This results in 38% of the thrust velocity V_{th} being ensured by the upper plate velocity V_{up}.

When the hanging wall velocity partially ensures the convergence (i.e., erosion is taken into account), maximum temperatures attained in and along the thrust zone are significantly rised (Fig. 9b). As an example, at 20 km depth, a 2 mm.yr^{-1} erosion velocity induces an increase of the maximum temperature of 80° for $\eta = 10^{20.25}$ Pa.s, of 110° for $\eta = 10^{20.5}$ Pa.s and of 140° for $\eta = 10^{20.75}$ Pa.s. This thermal jump increases with the viscosity. More generally, the maximum temperatures recorded along the thrust for a such erosion velocity ($Ve = 2$ mm.yr^{-1}) show an increase of 10 to 18% at 30 km depth, of 20 to 25% at 20 km depth and 19 to 32% at 10 km depth.Thermal influence of erosion is thus significantly intensified when shear heating is important, whereas it is almost negligible at low frictionnal heat production. However, if exhumation of the overthrusting rocks favours the thermal raise, its influence is inconsiderable with regard to the thermal perturbation intensity (Fig. 9a). Erosion velocities greater than 2 mm.yr^{-1} yield similar results and follow the same trend.

To sum up, concomitance of erosion processes with shear heating along a major thrust in realistic configurations (i.e., $Ve < Vb$) does not lead to significant variations in the

maximum thermal inversion intensity. But the maximum temperatures reached along the thrust are highly increased by several tens of degrees.

4. Discussion and conclusions

Through the present parametric study, we tested and compared the relative influences of the different processes and parameters involved in the thermal evolution in space and time of the continental crust around a major thrust zone:

(i)   the kinematic configuration of the thrust, i.e., the thrust dip angle, the convergence velocity, and the distribution of the thrust velocity on both sides of the shear zone (expressed here as the erosion velocity);

(ii)   the thermal rock properties controlling the heat diffusion across the rocks, i.e., the thermal conductivity, the heat capacity and the density;

(iii)   the heat sources, i.e., the basal mantle flux, the internal radiogenic heat production, including the accretion of radioactive material, and the mechanical energy converted into heat along the thrust during its activity (shear heating).

The initial kinematic configuration plays a major role. Whereas the thermal perturbation around the thrust increases in depth with increasing burial velocity of the downgoing plate, erosion localises the perturbation towards shallower depths of the crust and significantly increases its duration. However, for identical convergence velocities, any changes in the erosion velocity do not impact the intensity and the thickness of the thermal inversion contrary to the thermal conductivity. Nevertheless, whereas a limited and transient thermal inversion can be achieved in extreme kinematic configurations, inversion is never observed in the range of reasonable (reported from nature) values of these parameters. Among

all the processes and parameters tested, only shear heating allows the preservation of an intense thermal inversion through time under realistic kinematic schemes.

4.1. The thermal conductivity problem

The thermal conductivity, in the range of realistic values (i.e., between 2 and 4 $W.m^{-1}.K^{-1}$), has a major influence on the heat transfer by diffusion and on the initial geothermal gradient. Consequently, it strongly influences the local thermal gradient during the thrust activity, and when thermal inversion occurs, the intensity of this perturbation (Appendix C). As a rule, the initial thermal structure of the lithosphere is an important parameter to take into account in the models. However, tests comparing the thermal evolution of crusts with an identical initial temperature field but different thermal conductivities (the slope of the initial geotherm is thus balanced by the amount of mantle heat flux) attest to the significant effect of k on the intensity and duration of the thermal inversion (Appendix C).

Whereas the thermal conductivity (or thermal diffusivity) is generally considered to be constant in numerical models, it strongly depends on both the lithology and the physical environment, more particularly the temperature. The choice of the k values (Nabelek et al., 2010; Maierová et al., 2012) and corresponding empirical laws chosen in the numerical thermal models are capital and can lead to significant differences of the thermal behaviour of the lithosphere. For pressures higher than 100 MPa, the pressure effect is negligible and the thermal influence dominates with a strong decrease of k of ~ 1 $W.m^{-1}.K^{-1}$ for temperatures ranging from the surface to the base of the crust. Empirical thermo-dependence laws for various rock types were developed for atmospheric pressures. Empirical laws describing the evolution of k as a function of temperature under pressures higher than 100 MPa should give a better estimation of the thermal conductivity field in the crust for a given lithology. Furthermore, metamorphic reactions occurring along and across the thrust, the varying

amount of fluids in the rocks and the possible associated chemical changes linked to their circulation and/or chemical diffusion have also an impact on the evolution of the thermal conductivity of a given rock. These parameters are difficult to integrate in the models at present, but may have significant effects.

4.2. Shear heating, the key parameter

Shear heating, as defined in this paper and in the majority of other numerical models, considers that the whole energy required to overcome the fault friction is converted into thermal energy. However, this is a simplification and other energy transfers should be taken into account and their influence on the formation and preservation of the inverted thermal gradient tested. (i) The energy dissipated during a continuous deformation is not entirely converted into heat but can also be used to change the physical properties of the rock inside the sheared area (e.g., the rock microstructure; Brun and Cobbold, 1980). (ii) Metamorphic reactions occurring within and astride the shear zone can significantly consume or release heat (Oxburgh and Turcotte, 1976; Anderson et al., 1978; DeVore, 1983; Peacock, 1987a, b, 1990). (iii) Potential strain and gravitational energy (Kanamori and Rivera, 2006) can be transformed into pressurisation heat without displacement along the fault. Although these aspects should be taken into account in order to refine the general picture, they are not expected to modify the first-order message delivered by the modelling presented here.

Indeed, our results show that without shear heating, the occurence of thermal inversion requires extreme kinematic configurations (e.g., Kidder et al., 2013), is systematically transient (a few million years) and the inversion paroxysm is reached astride the thrust. In such a case, in order to preserve the trace of the thermal inversion in metamorphic parageneses (i.e., to avoid that any other metamorphic event significantly overprints the inverted record), exhumation of the whole sequence needs to be initiated during

the short period of time concerned by the inversion (some Myr) and to be extremely fast with a very high associated erosion velocity. On the other hand, under realistic kinematic configurations for intracontinental thrusts (up to 3 cm.yr^{-1}), shear heating is the only parameter which allows the preservation of the thermal inversion in time until the thermal steady state. It also significantly influences the spatial location and extent of the thermal inversion: (i) frictionnal heating along the thrust causes the localisation of the inversion area under rather than astride the thrust, within the uppermost levels of the lower plate, and (ii) the more frictionnal heat is produced, the thicker is the area affected by the thermal inversion leading to inversion zones up to tens of kilometers thick. The amount of heat produced depends on the local strain rate and the shear zone viscosity (Eq. (8)). The values of both parameters, and particularly the effective viscosity, strongly influence the crustal scale thermal perturbation, especially in terms of thermal inversion intensity.

The present study attests that shear heating is the key-parameter and allows to reproduce thermal features coming from natural inverted metamorphic sequences (Fig. 8). Both the high metamorphic peak temperatures (500-700°C at 8-11 kbar; e.g., Guillot, 1999; Pitra et al., 2010; Corrie and Kohn, 2011) and the thermal inversion intensities (generally comprised between 10 and 50°C.km^{-1}; e.g., Kohn, 2008; Pitra et al., 2010) can be reproduced. In parallel, our results suggest that the development and preservation of such inverted metamorphic zoning in realistic kinematic and thermal setting requires that the viscosity of the material involved has to be between 10^{20} and 10^{21} Pa.s.

4.3. Applicability to the Himalayan inverted metamorphism

The MCT in the Himalayas is characterised by a dip angle of 15° (e.g., Kaneko et al., 2003) and a downgoing velocity of the Indian plate of 2 cm.yr^{-1}. (e.g., Bilham et al., 1997; Lavé and Avouac, 2000). High metamorphic temperature peaks within the MCT reach 600 to

650°C and pressure peaks are of 8 to 11 kbar (e.g., Macfarlane, 1995; Guillot, 1999; Corrie and Kohn, 2011), corresponding to depths of about 30-40 km (assuming that these pressures correspond to lithostatic pressures). In agreement with the kinematical constraints, Fig. 8 shows that shear zone viscosity of $10^{20.5}$ to $10^{20.6}$ Pa.s is required to reproduce such maximum temperatures. The corresponding steady state thermal inversion intensity is 20 to 30°C.km^{-1}, hence matching the estimates extracted from Kohn (2008).

By taking into account erosion and accretion of radioactive rocks, as proposed by previous studies (e.g., Huerta et al., 1998; Bollinger et al., 2006) the range of consistent viscosities is slightly extended to $10^{20.35}$ to $10^{20.65}$ Pa.s and the corresponding maximum thermal inversion intensity spreads between 20 and 40°C.km^{-1} (Fig. 9). Whether or not accretion and surface denudation are considered, the thermal features of the inverted metamorphic zoning across the MCT can simply be reproduced by using shear heating and involving viscosities in the shear zone close to those commonly expected (e.g., Burg and Gerya, 2005).

Hence, our model, without pretending to explain the inverted metamorphism related to the MCT, shows that the downgoing of the Indian plate under the Himalayan belt with kinematical constraints from previous works associated with shear heating can reconcile: (i) the simultaneous increase of pressure and temperature conditions within the lower unit; (ii) the metamorphic temperature peaks recorded within the thrust zone as maximum temperatures reached and representative of the thermal steady state; (iii) the order of thermal inversion intensity and (iv) the location of such a thermal inversion mainly below and across the thrust zone. Furthermore it does not contradict the possible concomittance of accretion processes and suface denudation that, in a very lesser extent compared to shear heating, modify the characteristics of the thermal inversion.

Appendix A: Computation methods complements

Continental collision vs. continental subduction: The velocity field configuration of the downgoing plate beneath the first 30 km has a negligible influence on the thermal evolution around the thrust (Fig. A.1).

Interpolation computations between nodes end particles: They are realised by using a weight interpolation scheme (Gerya, 2010) between the Lagrangian particles and the Eulerian nodes. The interpolation from particles to nodes is realised on 1 cell by using at least 25 particles per cell. This constitutes a good compromise between the time needed for interpolation calculations and the generated numerical error (Yamato et al., 2012).

Advection computations: At each time step, the velocity field corresponding to the tectonic advection (both V_{lp} and V_{up}) is computed on each particle. The velocity direction of each particle is defined as parallel to the nearest segment of the thrust. In order to avoid a sharp variation of the velocity field on particles, the thrust profile was intentionally smoothed at the border of its slanted part (Fig. 1). The magnitude and the sign of each particle velocity are defined by its location relatively to the thrust. Particles are then advected by using the Runge-Kutta method. A Courant criterion maximising the advection to a half-cell by time step associated with the second-order Runge-Kutta method leads to an accurate advection while limiting the computation time (Fig. A.2). The differences between the fourth, third and second orders of the Runge-Kutta method are negligible.

Erosion computation: To simulate erosion, each particle advected above the topography is then numerically considered as part of the atmospheric domain by changing each one of the properties it carries. This way, erosion does not perturb the topography and consequently the crustal thickness that controls the vertical displacements linked to the isostatic balancing. The mass balance is assured by adding the corresponding amount of material laterally to the upper plate.

Thermal computations: heat diffusion equation (7) is solved by using the implicit finite difference method on the Eulerian grid. Then, the computed temperature difference on nodes ΔT between the current and the previous time step is interpolated from the grid to the particles. Finally, the new temperature is computed by adding the interpolated ΔT to the previous particle temperature. By ensuring the advection by particles, this method has the advantage of defining precisely the new temperature field directly on the particles.

Appendix B: Numerical model validation

Molnar and England (1990) and England and Molnar (1993), by using a series of simplifications, proposed mathematical derivations of the fundamental equations controlling the heat transfer in the lithosphere. This way, without additional heat sources, they defined the tectonic conditions for the occurrence of a thermal inversion on each point of the thrust such as:

$$\frac{Z_f \cdot V_{th} \cdot \sin(\theta)}{\pi \cdot \kappa} \geq 1 \tag{B.1}$$

where Z_f is the depth of the considered point on the fault. This can be used to provide the minimum depth Z_{min} where thermal inversion appears:

$$Z_{min} = \frac{\pi \cdot \kappa}{V_{th} \cdot \sin(\theta)} = \frac{\pi \cdot \kappa}{Vz} \tag{B.2}$$

Considering a point in the downgoing plate located at the thrust front, it will reach the depth Z_{min} after a time tz_{min}:

$$tz_{\min} = \frac{Z_{\min}}{Vz} = \frac{\pi \cdot \kappa}{Vz^2} \qquad (B.3)$$

Whereas England and Molnar considered θ constant along the entire slanted part of the fault, θ represents here the maximum dip angle of the thrust and an exact fit with the analytical solutions (B.2) and (B.3) cannot be expected and the thermal inversion is slightly underestimated.

The numerical minimum depth Z_{min} and start time t_{min} of the thermal inversion as a function of V_{th} and θ show a good agreement with the general trend of the analytical values given by or deduced from England and Molnar (1993) (Fig. B.1a, c). This consistency is confirmed by the linear regressions (Fig. B.1b, d) resulting from the set of numerical values. In spite of an overestimation of the minimum depth Z_{min} of about 5 km, the slope of the linear regression law between Z_{min} and Vz^{-1} is very close to the coefficient $\pi \cdot \kappa$ from Eq. (B.2) (Fig. B.1b). In the same way, the numerical times t_{min} show also a good agreement with the trend defined by the analytical solutions for tz_{min} (Eq. (B.3) and Fig. B.1c, d). Shifts between the analytical laws and linear regressions are essentially due to the smoothed thrust profile we used (Fig. 1).

Advection effects on the thermal evolution within a thrust zone can be thus described as a function of the vertical component of the thrust velocity Vz (Fig. 1). In Fig. B.1e, g, the results for a range of numerical simulations with different (Vz, k) combinations are treated in the same way as previously. Even if the slopes a relative to the linear regression laws corresponding to the minimum depth Z_{min} and time t_{min} (Fig. B.1f, h) of the beginning of the thermal inversion are rather far from the coefficient π predicted by England and Molnar (1993) (Eq. (B.2) and (B.3)), both the high similarity between our two regression slopes a and the very good correlation coefficients r confirm the tendencies of the analytical equations.

Appendix C: Rock thermal properties, mantle heat flux and radiogenic heat production effects

Heat capacity Cp crustal scale thermo-dependence law, from Whittington et al. (2009) (T in K):

$$\begin{cases} Cp_{crust}(T < 846K) = 899.54 + 0.3864 \cdot T - 2.25 \cdot 10^{-5} \cdot T^{-2} \\ Cp_{crust}(T > 846K) = 1034.0 + 0.1456 \cdot T - 21.59 \cdot 10^{-5} \cdot T^{-2} \end{cases} \tag{C.1}$$

Thermal conductivity k thermo-dependence laws as a function of the lithology, from Zoth and Hänel (1988) and Clauser and Huenges (1995) (T in °C):

$$\begin{cases} k_{crust}(T) = k_{metamorphic}(T) = \dfrac{705}{T + 350} + 0.75 \\ k_{mantle}(T) = k_{ultra-basic}(T) = \dfrac{1293}{T + 350} + 0.73 \end{cases} \tag{C.2}$$

Acknowledgments

References

Abd El-Naby, H., Frisch, W., Hegner, E., 2000. Evolution of the Pan-African Wadi Haimur metamorphic sole, Eastern Desert, Egypt. Journal of Metamorphic Geology, 18(6), 639-651.

Abdulagatov, I.M., Emirov, S.N., Abdulagatoca, Z.Z., Askerov, S.Y., 2006. Effect of Pressure and Temperature on the Thermal Conductivity of Rocks. Journal of Chemical and Engineering Data, 51(1), 22-33.

Anderson, R.N., DeLong, S.E., Schwarz, W.M., 1978. Thermal model of subduction with dehydration in the downgoing slab. Journal of Geology, 86, 731-739.

Andreasson, P.G., Lagerblad, B., 1980. Occurrence and significance of inverted metamorphic gradients in the western Scandinavian Caledonides. Journal of the Geological Society, 137(3), 219-230.

Arenas, R., Rubio Pascual, F.J., Diaz Garcia, F., Martinez Catalan, J.R., 1995. High-pressure micro-inclusions and development of an inverted metamorphic gradient in the Santiago Schists (Ordenes Complex, NW Iberian Massif, Spain): evidence of subduction and syncollisional decompression. Journal of Metamorphic Geology, 13(2), 141-164.

Arita, K., 1983. Origin of the inverted metamorphism of the lower Himalayas, Central Nepal. Tectonophysics, 95(1–2), 43-60.

Ballèvre, M., Bosse, V., Ducassou, C., Pitra P., 2009. Palaeozoic history of the Armorican Massif : Models for the tectonic evolution of the suture zones. C.R. Geoscience, 341, 174-201.

Beaumont, C., Jamieson, R.A., Nguyen, M.H., Lee, B., 2001. Himalayan tectonics explained by extrusion of a low-viscosity crustal channel coupled to focused surface denudation. Nature, 414(6865), 738-742.

Beaumont, C., Jamieson, R.A., Nguyen, M.H., Medvedev, S., 2004. Crustal channel flows: 1.Numerical models with applications to the tectonics of the Himalayan-Tibetan orogen. Journal of Geophysical Research, 109, B06406.

Bilham, R., Larson, K., Freymueller, J., 1997. GPS measurements of present-day convergence across the Nepal Himalaya. Nature, 386(6620), 61-64.

Bollinger, L., Henry, P., Avouac, J.P., 2006. Mountain building in the Nepal Himalaya: Thermal and Kinematic model. Earth and Planetary Science Letters, 244, 58-71.

Brun, J.P., Cobbold, P.R., 1980. Strain heating and thermal softening in continental shear zones: a review. Journal of Structural Geology, 2 (1/2), 149-158.

Brunel, M., Kienast, J.R., 1986. Etude pétro-structurale des chevauchements ductiles himalayens sur la transversale de l'Everest-Makalu (Népal oriental). Canadian Journal of Earth Sciences, 23, 1117-1137.

Burg, J.P., Leyreloup, A., Marchand, J., Matte, P., 1984. Inverted metamorphic zonation and large-scale thrusting in the Variscan Belt: an example in the French Massif Central. Geological Society, London, Special Publications, 14(1), 47-61.

Burg, J.P., Gerya, T.V., 2005. The role of viscous heating in Barrovian metamorphism of colli- sional orogens: thermomechanical models and application to the Lepontine Dome in the Central Alps. Journal of Metamorphic Geology, 23, 75-95.

Burg, J.P., Schmalholz, S.M., 2008. Viscous heating allows thrusting to overcome crustal-scale buckling: numerical investigation with application to the Himalayan syntaxes. Planetary Science Letters, 274, 189-203.

Caddick, M.J., Bickle, M.J., Harris, N.B.W., Holland, T.J.B., Horstwood, M.S.A., Parrish, R.R., Ahmad, T., 2007. Burial and exhumation history of a Lesser Himalayan schist: Recording the formation of an inverted metamorphic sequence in NW India. Earth and Planetary Science Letters, 264, 375-390.

Camiré, G., 1995. Development of inverted metamorphic gradient in the internal domain of the Taconian belt, Gaspé Peninsula. Canadian Journal of Earth Sciences, 32, 37-51.

Carter, N.L., Tsenn, M.C., 1987. Flow properties of continental lithosphere. Tectonophysics, 136(1–2), 27-63.

Čermák, V., Rybach, L, 1982. Thermal conductivity and specific heat of minerals and rocks, in Landolt-Börnstein: Numerical Data and Functional Relationships in Science and Technology, New Series, Group V (Geophysics and Space Research), Volume Ia, (Physical Properties of Rocks), edited by G. Angenheister, Springer, Berlin-Heidelberg, 305-343.

Chester, J.S., Chester, F.M., Kronenberg, A.K., 2005. Fracture surface energy of the Punchbowl fault, San Andreas system. Nature, 437(7055), 133-136.

Clauser, C., Huenges, E., 1995. Thermal conductivity of rocks and minerals. AGU Reference Shelf 3 Rock Physics and Phase Relations. A Handbook of Physical Constants, 105-125.

Corrie, S.L., Kohn, M.J., 2011. Metamorphic history of the central Himalaya, Annapurna region, Nepal, and implications for tectonic models. Geological Society of America Bulletin, 123(9-10), 1863-1879.

Crough, S.T., 1977. Isostatic rebound and power-law flow in the asthenosphere. Geophysical Journal of the Royal Astronomical Society, 50(3), 723-738.

DeVore, G.W., 1983. Relations between subduction, slab heating, slab dehydration and continental growth. Lithos, 16(4), 255-263.

England, P.C., Thompson, A.B., 1984. Pressure-temperature-time paths of regional metamorphism. I. Heat transfer during the evolution of regions of thickened continental crust. Journal of Petrology, 25, 4, 894–928.

England, P., Molnar, P., 1993. The interpretation of inverted metamorphic isograds using simple physical calculations. Tectonics, 12(1), 145-157.

Frank, W., Hoinkes, G., Miller, C., Purtscheller, F., Richter, W., Thöni, M., 1973. Relations between metamorphism and orogeny in a typical section of the Indian Himalayas. TMPM Tschermaks Mineralogische und Petrographische Mitteilungen, 20(4), 303-332.

Gerya, T.V., 2010. Introduction to numerical geodynamic modelling, New York: Cambridge University Press.

Gibson, H.D., Brown, R.L., Parrish, R.R., 1999. Deformation-induced inverted metamorphic field gradients: an example from the southeastern Canadian Cordillera. Journal of Structural Geology, 21, 751-767.

Goetze, C., Evans, B., 1979. Stress and temperature in the bending lithosphere as constrained by experimental rock mechanics. Geophysical Journal of the Royal Astronomical Society, 59(3), 463-478.

Graham, C.M., England, P.C., 1976. Thermal regimes and regional metamorphism in the vicinity of overthrust faults: an example of shear heating and inverted metamorphic zonation from southern California. Earth and Planetary Science Letters, 31, 142-152.

Grujic, D., Casey, M., Davidson, C., Hollister, L.S., Kündig, R., Pavlis, T.L., Schmid, S.M., 1996. Ductile extrusion of the Higher Himalayan Crystalline in Bhutan : evidence from quartz microfabrics. Tectonophysics, 260, 21-43.

Guillot, S., 1999. An overview of the metamorphic evolution of central Nepal. In : "Geology of Nepal", eds Upreti B.N. and Le Fort P, Journal of Asian Earth Sciences, 17, 713-725.

Hacker, B.R., 1991. The role of deformation in the formation of metamorphic gradients: Ridge subduction beneath the Oman Ophiolite. Tectonics, 10(2), 455-473.

Harrison, T.M., Ryerson, F.J., Le Fort, P., Yin, A., Lovera, O.M., Catlos, E.J., 1997. A late Miocene-Pliocene origin for the central Himalayan inverted metamorphism. Earth and Planetary Science Letters, 146, E1-E7.

Harrison, T.M., Grove, M., Lovera, O.M., Catlos, E.J., 1998. A model for the origin of Himalayan anatexis and inverted metamorphism. Journal of Geophysical Research, 103(B11), 27017-27032.

Harrison, T.M., Grove, M., Lovera, O.M., Catlos, E.J., d'Andrea, J., 1999. The origin of Himalayan anatexis and inverted metamorphism : Models and constraints. Journal of Asian Earth Sciences, 17, 755-772.

Hartz, E.H., Podladchikov, Y.Y., 2008. Toasting the jelly sandwich : The effects of shear heating on lithospheric geotherms and strength. Geology, 36, 331-334.

Henry, P., Le Pichon, X., Goffé, B., 1997. Kinematic, thermal and petrological model of the Himalayas: constraints related to metamorphism within the underthrust indian crust and topographic elevation. Tectonophysics, 273(1–2), 31-56.

Hofmeister, A.M., 2007. High-Pressure Geoscience Special Feature: Pressure dependence of thermal transport properties. Proceedings of the National Academy of Sciences, 104(22), 9192-9197.

Horai, K., Susaki, J., 1989. The effect of pressure on the thermal conductivity of silicate rocks up to 12 kbar. Physics of the Earth and Planetary Interiors, 55(3–4), 292-305.

Hubbard, M.S., 1989. Thermobarometric constraints on the thermal history of the Main Central Thrust Zone and Tibetan Slab, eastern Nepal Himalaya. Journal of Metamorphic Geology, 7(1), 19-30.

Huerta, A.D., Royden, L.H., Hodges, K.V., 1996. The interdependence of deformational and thermal processes in mountain belts. Science 273, 637-639.

Huerta, A.D., Royden, L.H., Hodges, K.V., 1998. The thermal structure of collisional orogens as a response to accretion, erosion, and radiogenic heating. Journal of Geophysical Research - Solid Earth 103, 15287-15302.

Huerta, A.D., Royden, L.H., Hodges, K.V., 1999. The effects of accretion, erosion and radiogenic heat on the metamorphic evolution of collisional orogens. Journal of Metamorphic Geology 17, 349-366.

Jain, A.K., Manickavasagam, R.M., 1993. Inverted metamorphism in the intracontinental ductile shear zone during Himalayan collision tectonics. Geology, 21(5), 407.

Jamieson, R.A., 1986. P-T paths from high temperature shear zones beneath ophiolites. Journal of Metamorphic Geology, 4(1), 3-22.

Jamieson, R.A., Beaumont, C., Hamilton, J., Fullsack, P., 1996. Tectonic assembly of inverted metamorphic sequences. Geology, 24, 9, 839-842.

Jamieson, R.A., Beaumont, C., Medvedev, S., Nguyen, M.H., 2004. Crustal channel flows: 2. Numerical models with implications for metamorphism in the Himalayan-Tibetan orogen. Journal of Geophysical Research, 109, B06407.

Johnson, M.R.W., Strachan, R.A., 2006. A discussion of possible heat sources during nappe stacking: the origin of Barrovian metamorphism within the Caledonian thrust sheets of NW Scotland. Journal of the Geological Society, 163(4), 579-582.

Kanamori, H., Rivera, L., 2006. Energy Partitioning During an Earthquake. Geophysical Monograph, series 170, Earthquakes: Radiated Energy and the Physics of Faulting, 3-13.

Kaneko, Y., Katayama, I., Yamamoto, H., Misawa, K., Ishikawa, M., Rehman, H.U., Kausar, A.B., Shiraishi, K., 2003. Timing of Himalayan ultrahigh-pressure metamorphism: sinking rate and subduction angle of the Indian continental crust beneath Asia. Journal of Metamorphic Geology, 21(6), 589-599.

Kidder, S., Ducea, M.N., 2006. High temperatures and inverted metamorphism in the schist of Sierra de Salinas, California. Earth and Planetary Science Letters, 241, 422-437.

Kidder, S.B., Herman, F., Saleeby, J., Avouac, J.P., Ducea, M.N., Chapman, A., 2013. Shear hesating not a cause of inverted metamorphism. Geology, doi: 10.1130/G34289.1.

Kohn, M.J., 2008. P-T-t data from central Nepal support critical taper and repudiate large-scale channel flow of the Greater Himalayan sequence. Geological Society of America Bulletin, 120, 3/4, 259-273.

Kukkonen, I.T., Jokinen, J., Seipold, U., 1999, Temperature and pressure dependencies of thermal transport properties of rocks: implications for uncertainties in thermal lithosphere models and new laboratory measurements of high-grade rocks in the central Fennoscandian shield. Surveys in Geophysics, 20, 33-59.

Lachenbruch, A.H., Sass, J.H., 1980. Heat Flow and Energetics of the San Andreas Fault Zone. Journal of Geophysical Research, 85(B11), 6185-6222.

Lavé, J., Avouac, J.P., 2000. Active folding of fluvial terraces across the Siwaliks Hills, Himalayas of central Nepal. Journal of Geophysical Research, 105(B3), 5735-5770.

LeFort, P., 1975. Himalayas : The collided range – Present knowledge of the continental arc. American Journal of Science, 275(A), 1-44.

Maierová, P., Chust, T., Steinle-Neumann, G., Čadek, O., Čížková, H., 2012. The effect of variable thermal diffusivity on kinematic models of subduction. Journal of Geophysical Research, 117(B7).

Macfarlane, A.M., 1995. An evaluation of the inverted metamorphic gradient at Langtang National Park, Central Nepal Himalaya. Journal of Metamorphic Geology, 13(5), 595-612.

Mason, R., 1984. Inverted isograds at Sulitjelma, Norway: the result of shear-zone deformation. Journal of Metamorphic Geology, 2, 77-82.

Meissner, R., Mooney, W., 1998. Weakness of the lower continental crust: a condition for delamination, uplift, and escape. Tectonophysics, 296(1–2), 47-60.

Minear, J.W., Toksöz, M.N., 1970. Thermal regime of a downgoing slab. Tectonophysics, 10(1–3), 367-390.

Molnar, P., England, P., 1990. Temperatures, Heat Flux, and Frictional Stress Near Major Thrust Faults. Journal of Geophysical Research, 95(B4), 4833-4856.

Nabelek, P.I., Whittington, A.G., Hofmeister, A.M., 2010. Strain heating as a mechanism for partial melting and ultrahigh temperature metamorphism in convergent orogens:

Implications of temperature-dependent thermal diffusivity and rheology. Journal of Geophysical Research, 115(B12), B12417.

Osako, M., Ito, E., Yoneda, A., 2004. Simultaneous measurements of thermal conductivity and thermal diffusivity for garnet and olivine under high pressure. Physics of the Earth and Planetary Interiors, 143–144(0), 311-320.

Oxburgh, E., Turcotte, D., 1976. The physico-chemical behaviour of the descending lithosphere. Tectonophysics, 32(1–2), 107-128.

Pavlis, T.L., 1986. The Role of Strain Heating in the Evolution of Megathrusts. Journal of Geophysical Research, 91(B12), 12407-12422.

Peacock, S.M., 1987a. Creation and preservation of subduction-related inverted metamorphic gradients. Journal of Geophysical Research, 92(B12), 12763-12781.

Peacock, S.M., 1987b. Thermal effects of metamorphic fluids in subduction zones. Geology, 15(11), 1057.

Peacock, S.M., 1990. Numerical simulation of metamorphic pressure-temperature-time paths and fluid production in subducting slabs. Tectonics, 9(5), 1197.

Pitra, P., Ballèvre, M., Ruffet G., 2010. Inverted metamorphic field gradient towards a Variscan suture zone (Champtoceaux Complex, Armorican Massif, France). Journal of Metamorphic Geology, 28, p183-208.

Platt, J.P., 1975. Metamorphic and deformational processes in the Franciscan Complex, California: Some insights from the Catalina Schist terrane. Geological Society of America Bulletin, 86(10), 1337 -1347.

Ranalli, G., Murphy, D.C., 1987. Rheological stratification of the lithosphere. Tectonophysics, 132(4), 281-295.

Royden, H.L., 1993. The steady state thermal structure of eroding orogenic belts and accretionary prisms. Journal of Geophysical Research, 98, 4487-4507.

Ruppel, C., Hodges, K.V., 1994. Pressure-temperature-time paths from two-dimensional thermal models: Prograde, retrograde, and inverted metamorphism. Tectonics, 13, 17-44.

Scholz, C.H., 1980. Shear heating and the state of stress on faults. Journal of Geophysical Research, 85, 6174-6184.

Searle, M.P., Rex, A.J., 1989. Thermal model for the Zankstar Himalaya. Journal of Metamorphic Geology, 7, 127-134.

Seipold, U., 1992. Depth dependance of thermal transport properties for typical crustal rocks. Physics of the Earth and Planetary Interiors, 69, 299-303.

Seipold, U., 1995. The variation of thermal transport properties in the Earth's crust. Journal of Geodynamics, 20, 2, 145-154.

Seipold, U., 1998. Temperature dependance of thermal transport properties of crystalline rocks — a general law. Tectonophysics, 291(1–4), 161-171.

Shi, Y., Wang, C.Y., 1987. Two-dimensional modeling of the P–T–t paths of regional metamorphism in simple overthrust terranes. Geology, 15, 1048-1051.

Sinha-Roy, S., 1982. Himalayan main central thrust and its implications for Himalayan inverted metamorphism. Tectonophysics, 84(2-4), 197-224.

Stephenson, B.J., Waters, D.J., Searle, M.P., 2000. Inverted metamorphism and the Main Central Thrust : field relations and thermobarometric constraints from the Kishtwar Window, NW Indian Himalaya. Journal of Metamorphic Geology, 18, 571-590.

Štípská, P., Schulmann, K., 1995. Inverted metamorphic zonation in a basement-derived nappe sequence ; eastern margin of the Bohemian Massif. Geological Journal, 30, 385-413.

Toksöz, M.N., Minear, J.W., Julian, B.R., 1971. Temperature Field and Geophysical Effects of a Downgoing Slab. Journal of Geophysical Research, 76(5), 1113-1138.

Turcotte, D.L., Schubert, G., 2002. Geodynamics, 2nd edition. Cambridge University press.

Voosten, H.D., Schellschmidt, R., 2003. Influence of temperature on thermal conductivity, thermal capacity and thermal diffusivity for different types of rock. Physics and Chemistry of the Earth, 28, 499-509.

Waples, D., Waples, J., 2004. A review and evaluation of specific heat capacities of rocks, minerals, and subsurface fluids. Part 1: Minerals and nonporous rocks. Natural Resources Research, 13, 2, 97-122.

Watkins, K.P., 1985. Geothermometry and geobarometry of inverted metamorphic zones in the W central Scottish Dalradian. Journal of the Geological Society, 142(1), 157-165.

Whittington, A.G., Hofmeister, A.M., Nabelek, P.I., 2009. Temperature-dependent thermal diffusivity of the Earth's crust and implications for magmatism. Nature, 458, 319-321.

Williams, H., Smyth, W.R., 1973. Metamorphic aureoles beneath ophiolite suites and alpine peridotites; tectonic implications with west Newfoundland examples. American Journal of Science, 273(7), 594-621.

Yamato, P., Tartèse, R., Duretz, T., May, D.A., 2012. Numerical modelling of magma transport in dykes. Tectonophysics, 526-529, 97-109.

Zoth, G., Hänel R., 1988. Thermal conductivity. "Handbook of Terrestrial Heat Flows Density Determination", Hänel, R., Rybach, L., Stegena, L., K., Dordrecht, 449-468.

Figure Captions:

Fig. 1. a) Model setup showing the initial morphology, the imposed velocity field and the thermal boundary conditions. Lower and upper continental blocs are converging at fixed velocities of V_{lp} and V_{up} respectively. θ is the maximum thrust dip angle. The compensation depth for isostatic balancing corresponds to the base of the model. Both surface temperature and mantle heat flux q_{base} are constant. k corresponds to the thermal conductivity. Lateral heat flux are considered to be nil. Rx represents the ratio between the distance to the thrust front and the width of the area concerned by the slanted part of the thrust. b) Terminology of the velocity fields used in this study. V_{th}, Vb, Ve and Vz correspond to the convergence velocity, the burial velocity of the lower plate, the erosion velocity and the vertical component of the thrust velocity, respectively. Accretion is defined by the vertical accretion velocity a. In order to keep the thrust zone fixed with respect to the reference frame, accretion is simulated by imposing an horizontal accretion velocity a' to the entire model. The dashed line represents the theoretical active thrust shifting due to accretion.

Fig. 2. Thermal evolution along the thrust as a function of the vertical component Vz of the thrust velocity and the relative erosion velocity Ve. a) Vertical thermal gradient and isotherms along the thrust. b) Vertical thickness of the area affected by the thermal inversion at each point of the thrust.

Fig. 3. Thermal evolution along the thrust as a function of the vertical component Vz of the thrust velocity and the thermal conductivity k (a and b) and the mantle heat flux q_{base} (c and d). Erosion is switched off and no internal heat sources are taken into account. a) and c) Vertical thermal gradient and isotherms along the thrust. b) and d) Vertical thickness of the area affected by the thermal inversion at each point of the thrust.

Fig. 4. Empirical thermo-dependence laws for k for various lithologies. a) Seipold (1998). Fine lines show the variations of the uncertainty for each rock type as a function of temperature. b) Clauser and Huenges (1995), after the relation proposed by Zoth and Hänel (1988). Uncertainties are unknown. c) and d) Comparison of thermo-dependence laws illustrated in (a) and (b) for two rock types: basic (c) and acid (d). Grey band is the uncertainty from (a).

Fig. 5. a) Influence of the shear heating Hs on the spatial evolution of the geothermal gradient and isotherms, and on the location of thermal inversion. [Left] Without shear heating and under extreme kinematic conditions ($\theta = 30°$ and $V_{th} = 5$ cm.yr^{-1}). Thermal evolution 1 Myr after the thrust activity starting, i.e., at the maximum thermal inversion. [Right] Thermal evolution with shear heating at viscosity $\eta = 10^{20.5}$ Pa.s after 5 Myr, when the thermal steady state has been reached (kinematic conditions are: $\theta = 15°$ and $V_{th} = 2$ cm.yr^{-1}, i.e., $\dot{\varepsilon} = 6.34$. 10^{-13} s^{-1}). S is the cumulative shortening. b) Temporal evolution of the geothermal gradient along a vertical profile located in the center of the model ($Rx = 50$ %, Fig. 1) according to three different constant viscosities: $\eta = 10^{20}$ Pa.s, $\eta = 10^{20.25}$ Pa.s and $\eta = 10^{20.5}$ Pa.s. c) Corresponding thermal increment by shear heating along the thrust during its activity.

Fig. 6. Impact of shear heating on the thermal evolution along the thrust during the convergence as a function of strain rate $\dot{\varepsilon}$ and viscosity η. a) Vertical thermal gradient (colour scale) and isotherms (black lines) at 1 km under the thrust, i.e., close to the maximum thermal inversion for each vertical profile across the crust. b) Vertical thickness of the area affected by the thermal inversion on each point of the thrust.

Fig. 7. a) Maximum thermal inversion intensity reached beneath the thrust zone in presence of shear heating and after the thermal steady state has been reached (10 Myr). Mantle heat flux is set to 40 mW.m^{-2} and no radiogenic heating is considered such as the initial Moho temperature is 420˚C. The thrust dip angle is defined to 15˚. Results are given as a function of convergence velocity V_{th}, viscosity η and depths (10, 20 and 30 km). b) Maximum temperature. Hatched areas indicate the combinations (V_{th}, η) for which no thermal inversion occurs.

Fig. 8. Combination of maximum thermal inversion intensity and maximum temperature from results presented in Fig. 7 at 20 and 30 km depth. Ranges of values are selected with respect to the reported thermal characteristics of intracontinental inverted metamorphic sequences. Maximum temperatures are drawn for values of 500, 600 and 700˚C (continuous lines). Maximum inverted geothermal gradients are represented from 10 to 50˚C.km^{-1} (dashed lines). Dark green areas represent the combinations (V_{th}, η) for which both thermal characteristics are in the range of values considered as "realistic". Hatched areas indicate the combinations (V_{th}, η) for which no thermal inversion occurs.

Fig. 9. a) Maximum thermal inversion intensity and b) maximum temperature from the thrust zone in presence of shear heating, accretion processes and/or radiogenic heat production or surface denudation after 10 Myr (thermal steady state is reached). Results are given as a function of the viscosity η and are plotted for 20 km (dashed lines) and 30 km depth (continuous lines). The numerical simulations were realised at a convergence velocity V_{th} set to 2 cm.yr^{-1}, with a thrust dip angle $\theta = 15˚$ and a mantle heat flux $q_{base} = 40$mW.m^{-3}. The grey areas correspond to the ranges of inverted thermal gradients and metamorphic peak temperatures characterising natural intracontinental inverted metamorphic sequences (see

sections 3.5 and 3.6 for details about the radiogenic, accretion and erosion conditions). Hatched area in (a) delimits the range of geothermal gradients not inverted.

Fig. A.1. Comparison between two velocity field configurations: "Collision mode", in which the downgoing plate lies flat under the crustal part of the upper plate, and "Subduction mode", in which it subducts into the mantle without change of direction. Isostatic balance is switched off. In order to highlight the thermal characteristics differences between both models, computations were realised under extreme kinematic conditions: V_{th} = 5 cm.yr^{-1} and θ = 30˚. [top] Snapshots and corresponding isotherms (in ˚C) of both models after a 1 Myr convergence (amount of shortening S = 50 km), i.e., when the thermal inversion reached its paroxysm. [bottom] Differences of characteristic values of the thermal evolution along the thrust between the "Collision mode" and the "Subduction mode": temperature, vertical thermal gradient and thickness of the thermal inversion, respectively from left to right. For each characteristic value, the difference between both models is minor compared to the absolute values.

Fig. A.2. Influence of the computation mode of the velocity field on particles mode and of the Courant criterion on total advection. a) Initial test setup and corresponding velocity field. The dimensionless 2D-model represents a disc composed by regularly emplaced particles. The imposed velocity field is circular in order to make the disc rotate around its center. Time step is defined according to the Courant criterion applied on the maximum local velocity, i.e., on the disc border. For example, a Courant criterion of 3 thus maximises the advection to a third-cell by time step. A reference marker is localised on this border. Velocity field on particles was computed according to four different modes: on the one hand, direct computation is only characterised by linearly interpolating the velocity field from the nodes to the particles, while

on the other hand, advection is realised according to the Runge-Kutta approximations of order 2, 3 or 4. Tests were also realised for a range of particles amount, from 1 to 100 per cell. Number of particles does not impact on the effective advection. b) Offset after a complete revolution. Every test leads to a certain numerical error, i.e., the reference marker does not keep constant its distance to the disc center. While direct computation is characterised by a terminal offset of about 10 to 40 %, the Runge-Kutta methods allow a significant improvement of the particles advection leading to total offset of about 10^{-2} to 10^{-3} % for the order 2 and 3, and for less than 10^{-4} % for the order 4. In the present test, the offset is positive for the direct computation and the 2nd order of Runge-Kutta methods, i.e., the disc tends to dilate, whereas it is negative for the other two Runge-Kutta orders. This explains why the 2nd and 3rd orders are very similar in absolute. The Courant criterion also plays a main role in numerical advection. In the present test, increasing it with a factor 2 assures the reduction of the space error (offset) of a factor 2 for the simple computation, of a factor 8 for the Runge-Kutta methods of order 2 and 3, and of a factor 32 for the 4th order. c) Relative time of computations normalised to the maximum time (i.e., for the 4th order of the Runge-Kutta approximation, with a Courant criterion of 4 and 100 particles/cell). Results are given in percents. Time of computation linearly increases with the Courant criterion, with the amount of particles and also with the order of the used Runge-Kutta method. Even if there is an important gap between the calculation times of the direct computation and the 2nd order of the Runge-Kutta approximation, the benefit of space advection precision significantly prevails. The present test reveals an advection error (offset) of only 0.0098 % and an associated computation time more than 2 times lower than for the 3rd order and approximately 4 times better than for the 4th order. Consequently, these observations lead us to use a Courant criterion of 2 associated with the 2nd order of the Runge-Kutta method for a good compromise between the advection approximation and the computation time.

Fig. B.1. Role of the kinematic conditions (V_{th} and θ) and the thermal conductivity k: validation of the numerical model with respect to analytical developments. Erosion and accretion are switched off. Rock thermal properties are set to the reference values (Table 1). a) Minimum depth Z_{min} of thermal inversion reached during the thrust activity as a function of V_{th} and θ. Comparison between our numerical results (coloured circles) and the analytical solution from England and Molnar (1993) (Eq. (B.2)) (background). Small circles: real computed depth. Gray points correspond to the cases where no thermal inversion occurs. Large circles: real computed depth minored by 5.168 km (see text for details). b) Numerical Z_{min} as a function of Vz^{-1} (coloured circles). The linear regression is represented by the continuous line. The straight dashed line corresponds to the analytical linear law from England and Molnar (1993). c) Time t_{min} of the thermal inversion start as a function of V_{th} and θ. Comparison between our numerical results (coloured circles) and the analytical solution for tz_{min} developed after England and Molnar (1993) (Eq. (B.3)) (background). d) Numerical t_{min} as a function of Vz^{-2} (coloured circles). The linear regression is represented by the continuous line. The dashed straight line corresponds to the analytical linear law after England and Molnar (1993). e) Minimum depth Z_{min} in function of Vz and k. Comparison between our numerical results (coloured circles) and the analytical solution from England and Molnar (1993) (Eq. (B.2)) (background). Small circles: real computed depth. Gray points correspond to the cases where no thermal inversion occurs. Large circles: real computed depth minored by 5.168 km (see b). f) Numerical Z_{min} as a function of $\kappa.Vz^{-1}$ (coloured circles). The linear regression is represented by the continuous line. The dashed straight line corresponds to the analytical linear law from England and Molnar (1993).g) Time t_{min} of the thermal inversion start in function of Vz and k. Comparison between our numerical results (coloured circles) and the analytical solution for tz_{min} developed after England and Molnar (1993) (Eq. (B.3))

(background). h) Numerical t_{min} as a function of $\kappa.Vz^{-2}$ (coloured circles). The linear regression is represented by the continuous line. The dashed straight line corresponds to the analytical linear law after England and Molnar (1993).

Fig. B.2. Thermal evolution for an extreme kinematic setting: $V_{th} = 5$ cm.yr^{-1}, $\theta = 30°$. a) Evolution during the thrust activity: geometry of the lithosphere and isotherms (left) and vertical thermal gradient (right). S is the amount of shortening. b) Temporal evolution of the geothermal gradient along 3 profiles corresponding to Rx = 25 %, 50 % and 75 % (Fig. 1). Steady state is more rapidly reached in the shallowest part of the thrust, and thermal inversion duration in depths does not exceed 6 Myrs.

Fig. C.1. Rock thermal properties and mantle heat flux effects on the thermal inversion under extreme kinematic conditions ($V_{th} = 5$ cm.yr^{-1}, $\theta = 30°$). a) and e) Heat capacity Cp effects. b) and f) Thermal conductivity effects. c) and g) Mantle heat flux q_{base} effects. d) and h) Combined k and q_{base} effects, considering identical initial geotherms. [Top] Thick lines are geotherms after a 1 Myr convergence (amount of shortening $S = 50$ km) along the central crustal profile, i.e., $Rx = 50$ % (Fig. 1). Fine lines represent the corresponding initial geotherms. [Bottom] Evolution of the maximal intensity of the thermal inversion reached along the thrust. Solid blue lines (and numbers) show the variation of Cp and k with depth (and hence with temperature) for the initial geotherm. Dashed blue lines are the results of the corresponding simulations.

Fig. C.2. Radiogenic heat production effects on the thermal inversion under extreme kinematic conditions: $V_{th} = 5$ cm.yr^{-1} and $\theta = 30°$. a) and d) Surface radiogenic heat production Q_0 effects. b) and e) Specific depth z_r effects. c) and f) Combined Q_0 and z_r effects such as the initial mean crustal radiogenic heat productions are the same. [Top] Thick lines

are geotherms after a 1 Myr convergence (amount of shortening $S = 50$ km) along the central crustal profile, i.e., $Rx = 50$ % (Fig. 1). Fine lines represent the corresponding initial geotherms. [Bottom] Evolution of the maximal intensity of the thermal inversion reached along the thrust.

Table Captions:

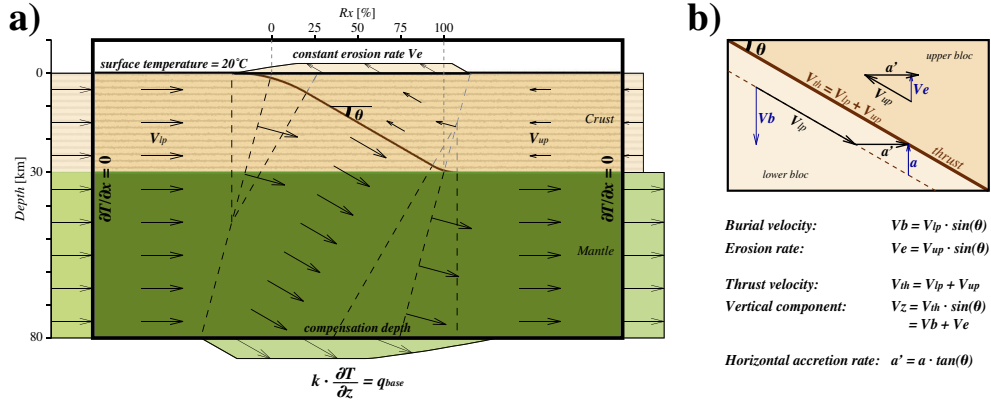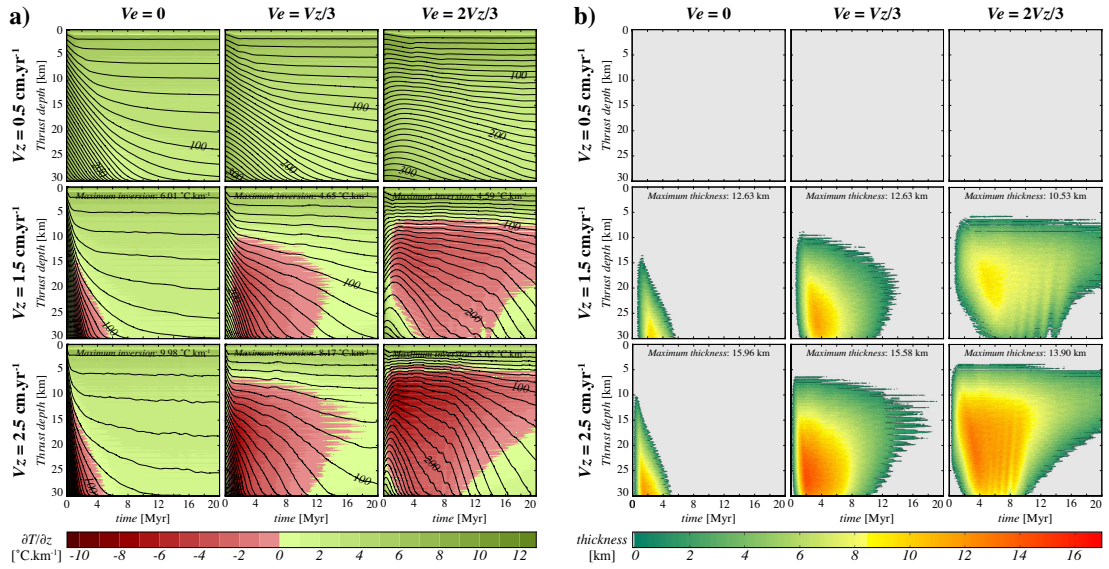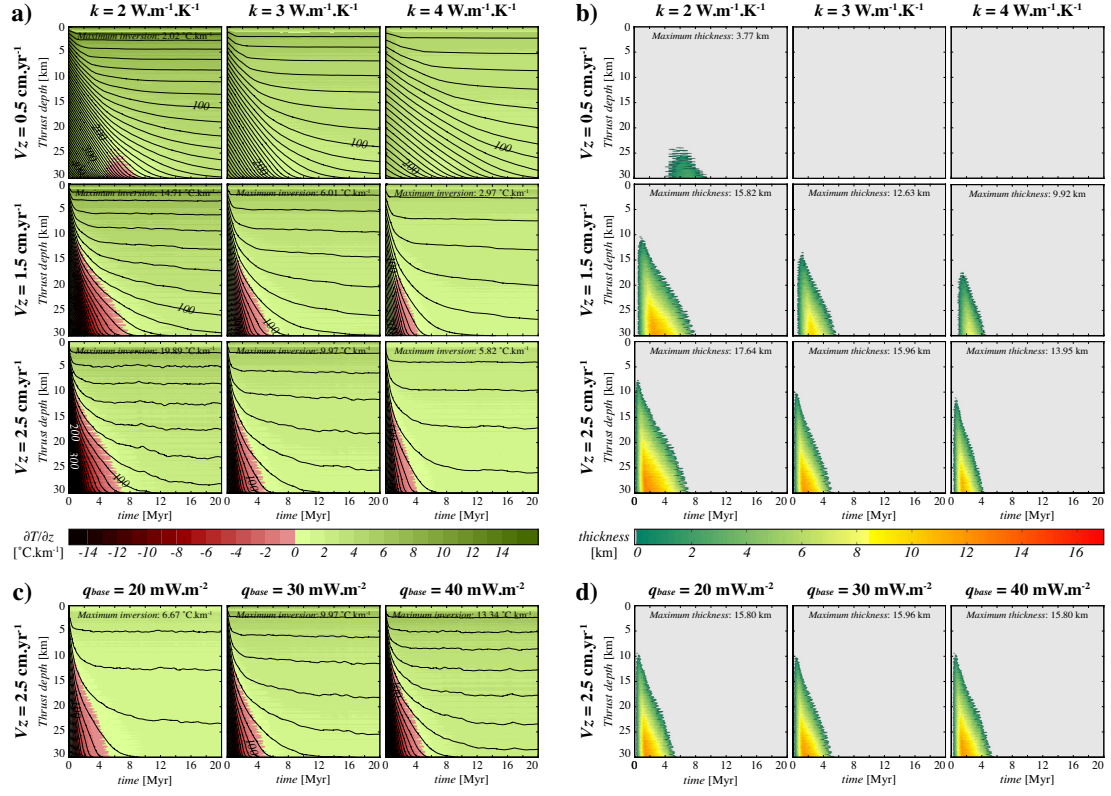**Table 1.** Parameters tested in the model.
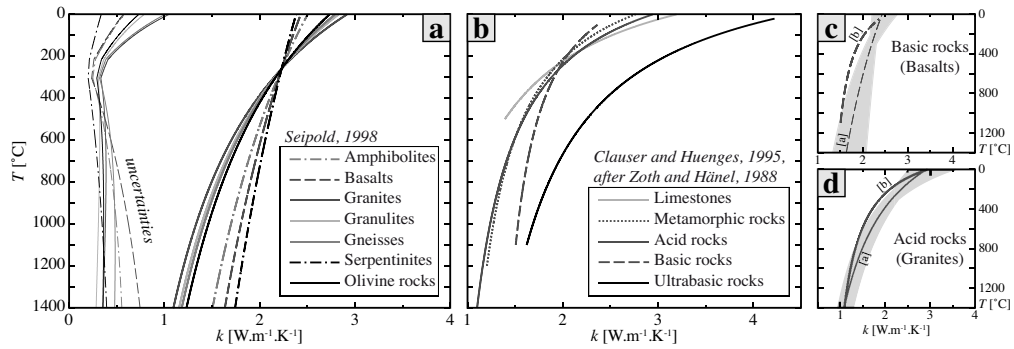
Figure 1

Figure 2

Figure 3

Figure 4

54

Figure 5

a) Spatial evolution of the geothermal gradient [°C.km⁻¹] and isotherms [°C]

b) Temporal evolution of the geothermal gradient [°C.km⁻¹] - *Rx* = 50%

c) Amount of warming along the thrust by shear heating
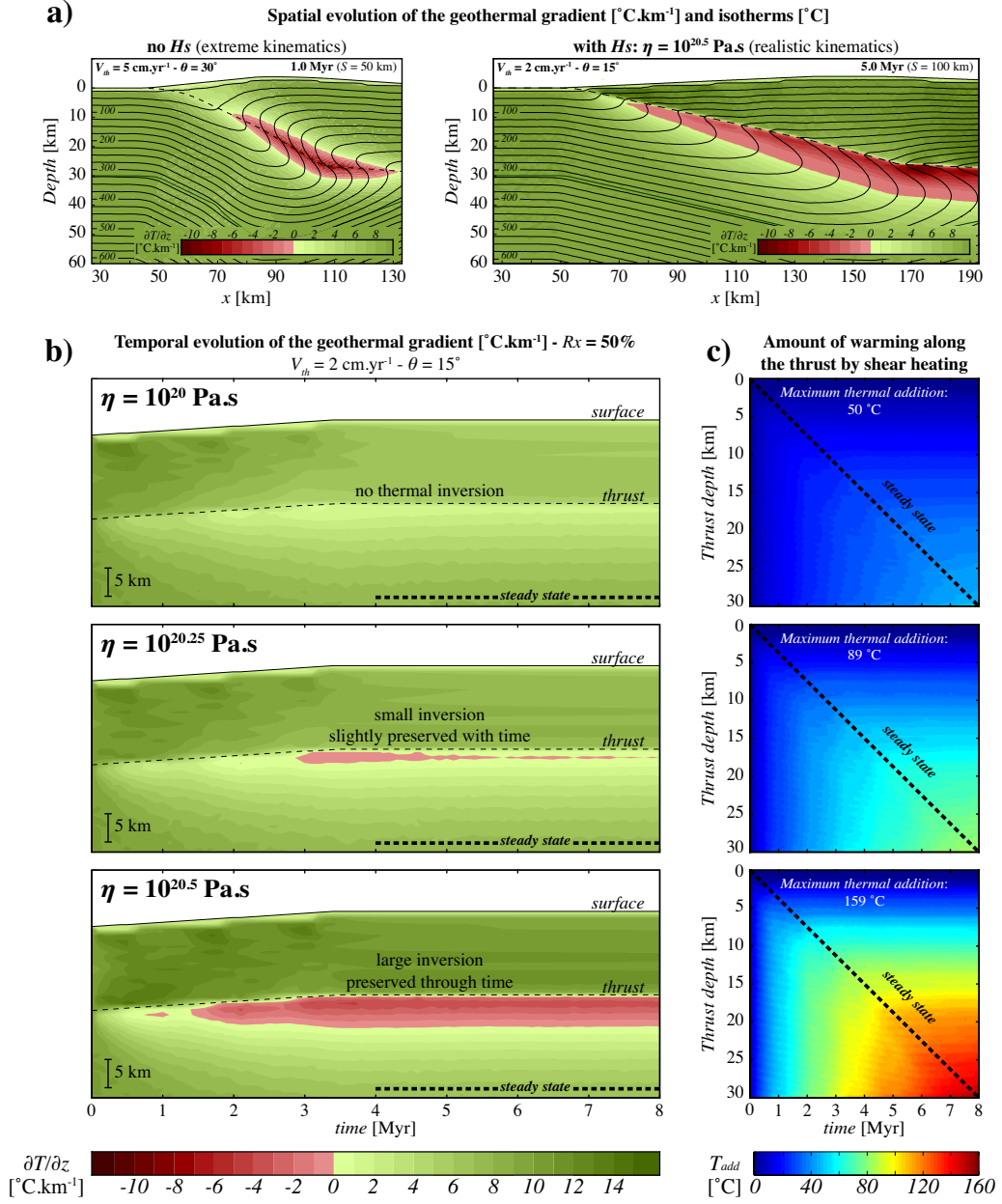
Figure 6

Figure 7

Figure 8

depth = 20 km   depth = 30 km

maximum TI intensities $\in [10; 50]°C.km^{-1}$

maximum temperatures $\in [500; 700]°C$

both thermal characteristics are in the ranges of the true values

only one of the two thermal characteristics is in the ranges of the true values

Figure 9

a) **maximum thermal inversion intensity**

thermal and kinematic conditions

Only shear heating
(without accretion or radiogenic heat production or erosion)

Shear heating and accretion
(without radiogenic heat production or erosion)

$a = 1$ mm.yr^{-1}

$a = 2$ mm.yr^{-1}

b) **maximum temperature**

Shear heating, accretion and radiogenic heat production
(without surface denudation)
$a = 2$ mm.yr^{-1}, $Q_0 = 2$ µW.m^{-3}

$z_r = 15$ km

$z_r = 30$ km

Shear heating and erosion
(without accretion or radiogenic heat production)
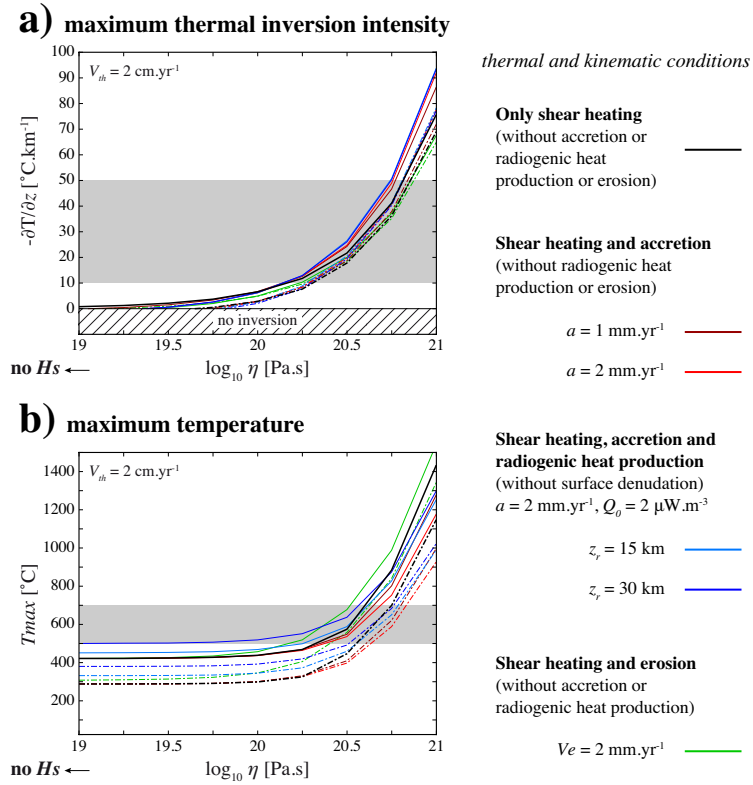
$Ve = 2$ mm.yr^{-1}
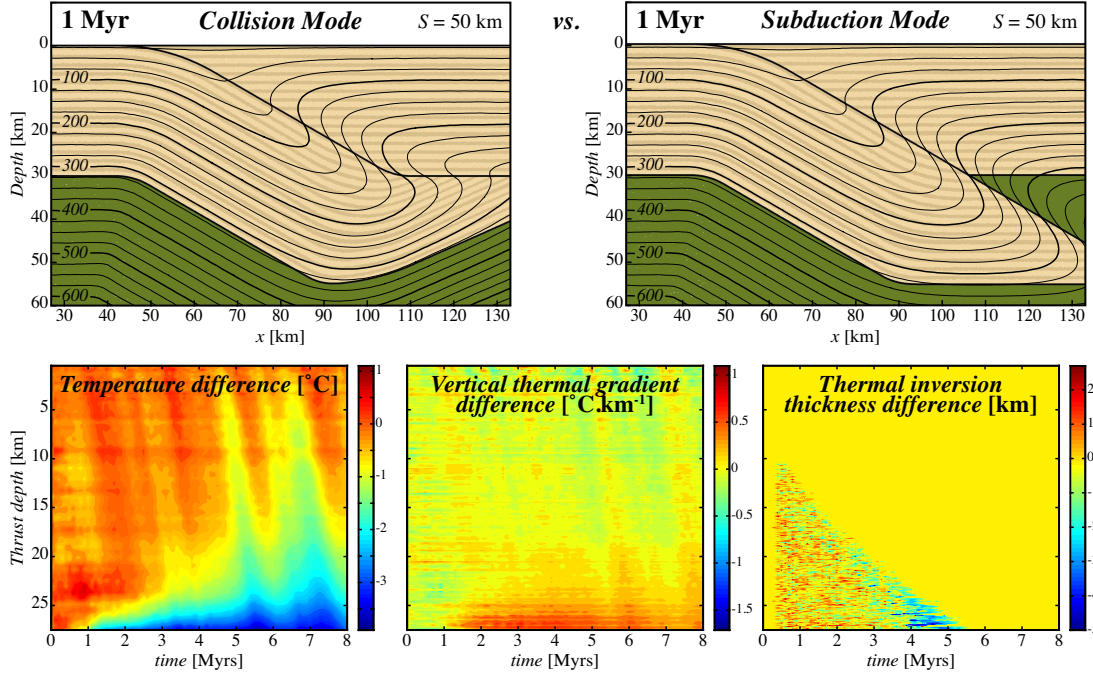
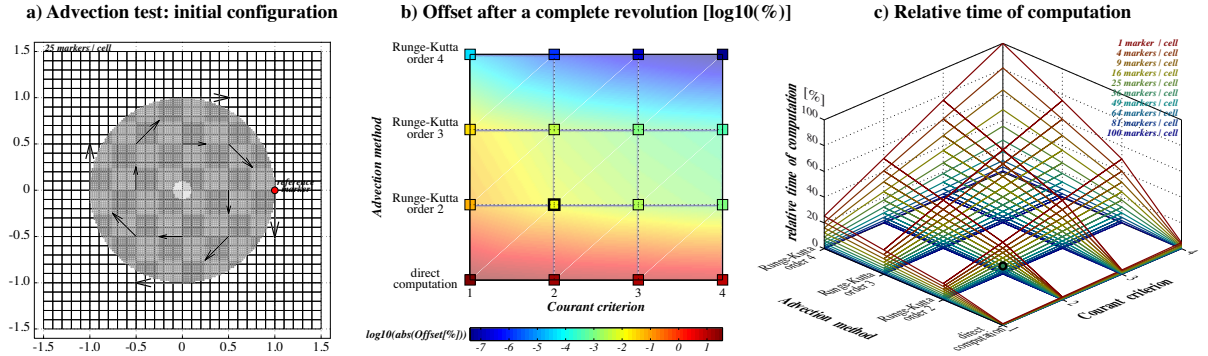Figure 10: *Appendix Figure A.1*

Figure 11: *Appendix Figure A.2*
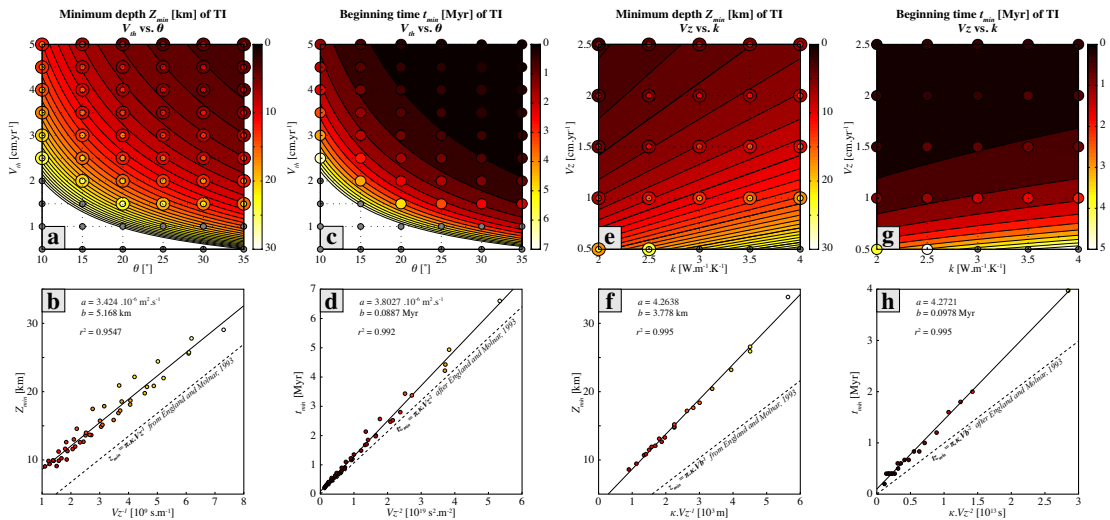

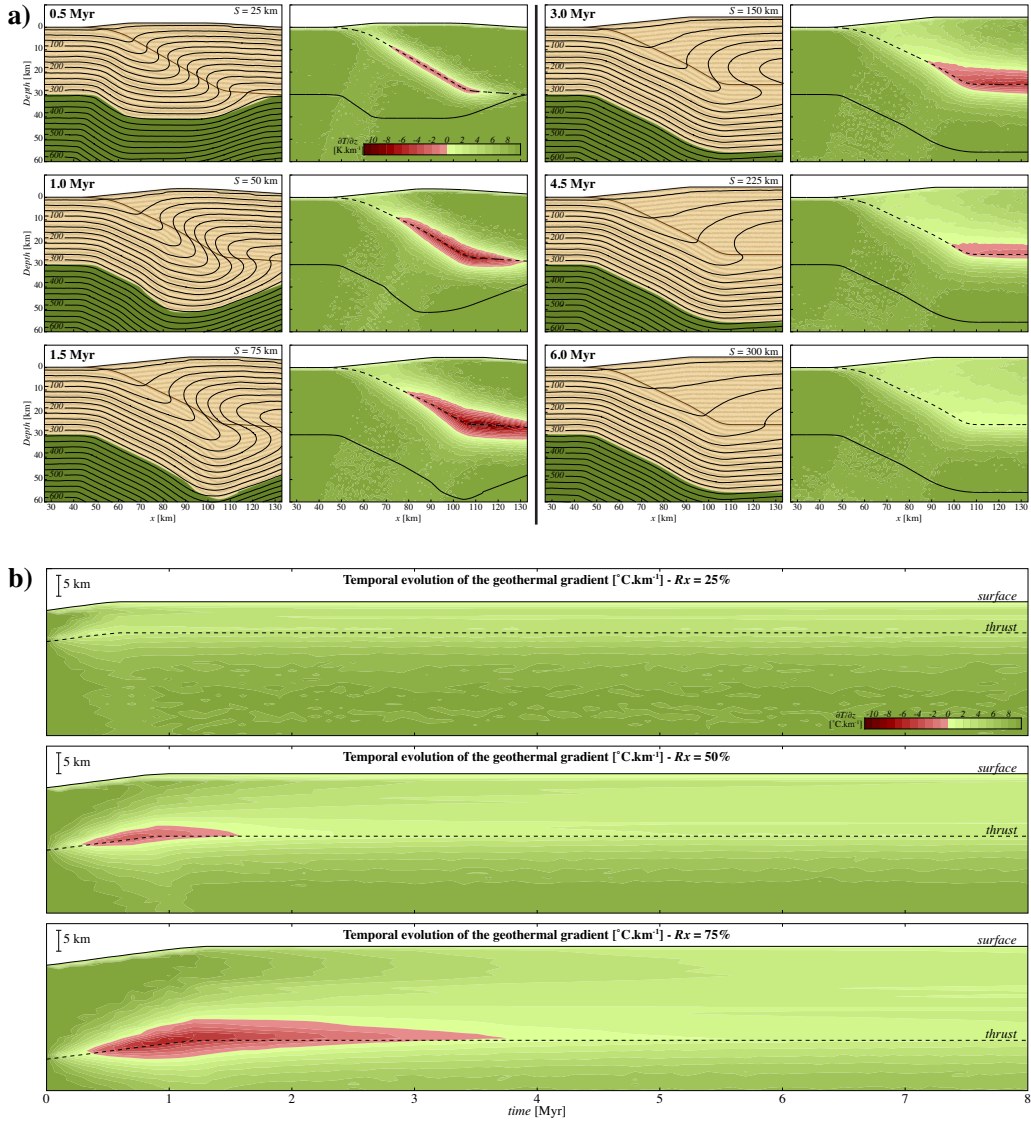Figure 12: *Appendix Figure B.1*

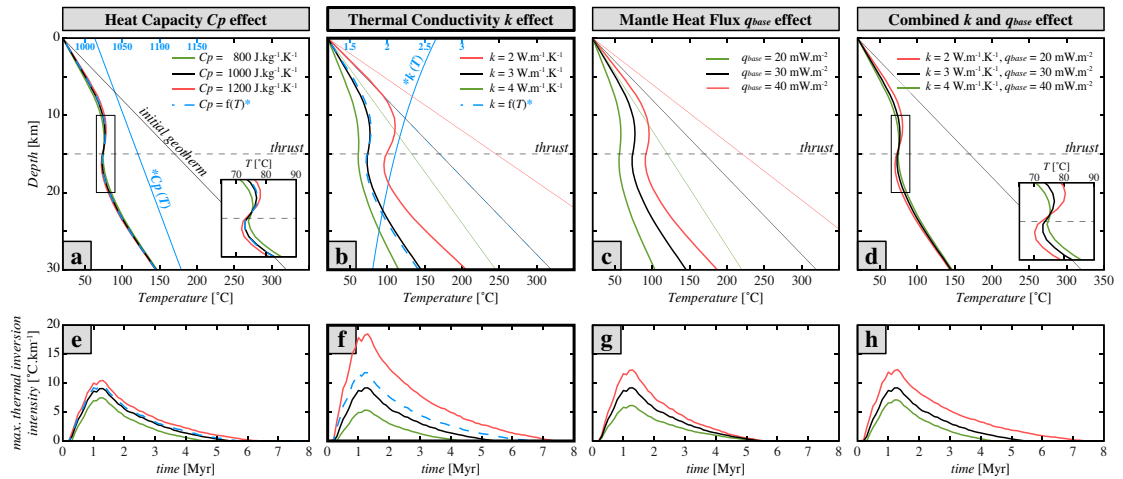Figure 13: *Appendix Figure B.2*

Figure 14: *Appendix Figure C.1*

Figure 15: *Appendix Figure C.2*

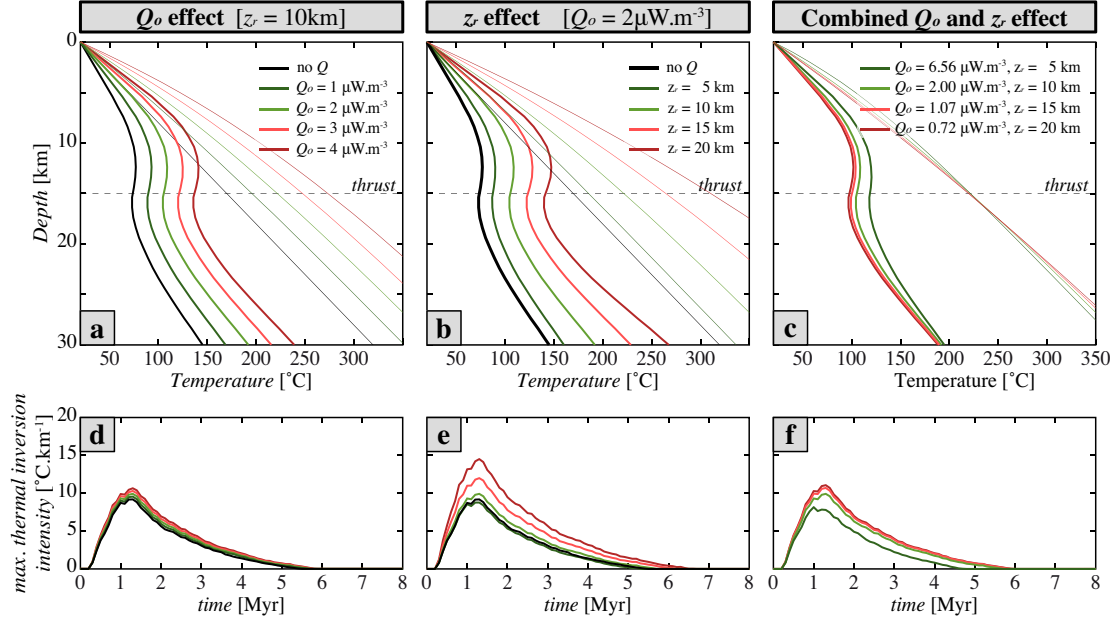Figure 16: *Table 1*

Symbol	Parameter	Range of tested values	Unit
Kinematic parameters:			
θ	Thrust dip angle	10 - 35	°
V_{th}	Thrust velocity (convergence rate)	0.5 - 5	cm.yr^{-1}
Vz	Vertical component of V_{th}	$V_{th} \cdot \sin(\theta)$	cm.yr^{-1}
V_{lp}	Lower plate velocity	0.5 - 5	cm.yr^{-1}
Vb	Burial velocity	$V_{lp} \cdot \sin(\theta)$	cm.yr^{-1}
V_{up}	Upper plate velocity	$V_{th} - V_{lp}$	cm.yr^{-1}
Ve	Erosion rate	$V_{up} \cdot \sin(\theta)$	cm.yr^{-1}
a	Vertical accretion rate	0 - 0.2	cm.yr^{-1}
a'	Horizontal accretion rate	$a' \cdot \tan(\theta)$	cm.yr^{-1}
Rock thermal properties:			
ρc	Crust density	2800	kg.m^{-3}
ρm	Mantle density	3300	kg.m^{-3}
Cp	Heat capacity	800 - 1200	J.kg^{-1}.K^{-1}
k	Thermal conductivity	2 - 4	W.m^{-1}.K^{-1}
κ	Thermal diffusivity in the crust	$k/(\rho c.Cp)$	m^2.s^{-1}
Heat sources:			
q_{base}	Mantle heat flux	20 - 40	mW.m^{-2}
Q	Radiogenic heat production		µW.m^{-3}
Q_0	Surface radiogenic heat production	0 - 4	µW.m^{-3}
z_r	Specific depth where $Q = Q_0.e^{-1}$	5 - 20	km
Hs	Shear heating		µW.m^{-3}
η	Thrust effective viscosity	$10^{19} - 10^{21}$	Pa.s